University of Twente

Technical Medicine

Thesis Subject

Electro-mechanical resynchronisation therapy with a smart material in patients with heart failure: an experimental study

Karlijn Aarnink

27 October 2017

University of Twente
Medical supervisor: Prof. J.G. Grandjean MD PhD
Medical supervisor: S.A.M. Said MD PhD
Technical supervisor: J.M.J. Paulusse PhD
Process supervisor: P.A. van Katwijk MSc
Practical supervisor: F.R. Halfwerk MD MSc

UNIVERSITY OF TWENTE.

Thorax Centrum Twente

MST

zgt

Abstract

Introduction: Heart failure (HF), a clinical syndrome, is increasingly prevalent in West-European countries. The purpose of treatment in patients with HF is to improve their clinical condition, quality of life, prevent hospital admission and reduce mortality. A select group of HF patients with reduced ejection fraction (HFrEF) are eligible for cardiac resynchronisation therapy (CRT), which can improve refilling and contraction pattern of both ventricles. However, 30 - 40% of patients who are treated with CRT remain non-responders. The aim of this study is to investigate if a shape memory alloy (SMA) is able to support and strengthen the pump function of the heart and create an improvement in ejection fraction (EF) of 5%.
Method: A paediatric ventilation balloon was used as a heart model. Flexinol®, an SMA, was placed around the heart model and activated by using pulse width modulation (PWM) technique to determine the influence of diameter, configuration, insulation and variables of PWM on volume displacement. Furthermore, temperature of the SMA and pressure within the heart model was measured with a thermal image camera and a fabricated pressure sensor, respectively.
Results: An SMA with a diameter of 0.38 mm, which was placed in a spiral shape and activated with a duty cycle of 80% and a frequency of 50/min gave the highest volume displacement. A silicone tube insulated the SMA-wire well. Maximum achieved EF was 3.5%.
Conclusion: This study confirmed that volume displacement was successfully demonstrated in a static heart model by activation of SMA-wires around the model. It gave furthermore insight in the influence of several factors (i.e. configuration, duty cycle, frequency, pulse intervals, diameter and insulation) on the activation of SMA-wires and corresponding volume displacement. Recommendations for further optimisation of experiments were made.

Highlights

- A spiral shaped SMA reached the highest displaced volume;
- A maximal EF of 3.5% was reached;
- Silicone tube insulated the SMA-wire and retained heat;
- Activation of five SMA-wires caused a pressure of 10.3 mmHg in the static heart model.

Contents

Acronyms

ACE angiotensin-converting-enzyme.

BNP B-type natriuretic peptide.

CO cardiac output.

CRT cardiac resynchronisation therapy.

DCM dilated cardiomyopathy.

EDPVR end-diastolic pressure-volume relation.

EDV end-diastolic volume.

EF ejection fraction.

ESPVR end-systolic pressure-volume relation.

ESV end-systolic volume.

HF heart failure.

HFmrEF heart failure with mid-range ejection fraction.

HFpEF heart failure with preserved ejection fraction.

HFrEF heart failure with reduced ejection fraction.

HR heart rate.

ICD implantable cardioverter defibrillator.

IVC inferior vena cava.

LA left atrium.

LV left ventricle.

LVAD left ventricular assist device.

LVEF left ventricular ejection fraction.

NiTi nickel-titanium.

NT-proBNP NT-pro B-type natriuretic peptide.

NYHA New York Heart Association.

PWM pulse width modulation.

RA right atrium.

RV right ventricle.

SE superelasticity.

SMA shape memory alloy.

SME shape memory effect.

SMP shape memory polymer.

SMPU smart memory polyurethane.

SV stroke volume.

SVC superior vena cava.

TAVI transcatheter aortic valve implantation.

1 Introduction

1.1 The Heart

The heart is an important organ of the human body and usually as big as someone's fist. Its main function is to pump blood to tissues and organs, to provide them with the necessary oxygen and nutrients. Heart failure (HF) influences the heart function and can have a major impact on quality of life. Additional information about the anatomy, physiology and pathophysiology of the heart can be found in Appendix A, Chapter 6.

1.2 Heart Failure

HF is a clinical syndrome which is caused by a decreased pump function of the heart and is characterised by symptoms, such as dyspnoea, tiredness and oedema, in rest or during exercise [1]. The New York Heart Association (NYHA) classification is the most widely used classification to describe the severity of the clinical symptoms of patients with HF, see Table 1. This NYHA-classification has a prognostic value and was demonstrated to be useful in clinical practice [2–4].

In West-European countries, HF is increasingly prevalent, affecting 1% - 2% of the total population and an incidence of approximately 5-10 per 1000 people per year [6]. In the Netherlands, 1% (± 130.000) of the adult population suffers from HF, which will increase to 195.000 in 2025. A Dutch research study reported 1, 2 and 5-year survival rates of 65%, 51% and 35%, respectively. Furthermore, risk of death was much higher in patients with HF compared to age and gender matched population [7].

Table 1: Classification of patients with heart disease, according to the New York Heart Association (NYHA) classification [5].

Class	Symptoms
I	No limitation of physical activity; normal physical activity does not cause undue fatigue, palpitation or dyspnoea.
II	Slight limitation of physical activity; comfortable at rest, but ordinary physical activity results in fatigue, palpitation or dyspnoea.
III	Severe limitation of physical activity; no or almost no symptoms at rest, but less than ordinary activity causes fatigue, palpitation, or dyspnoea.
IV	Unable to carry on any physical activity without discomfort. Symptoms also present at rest.

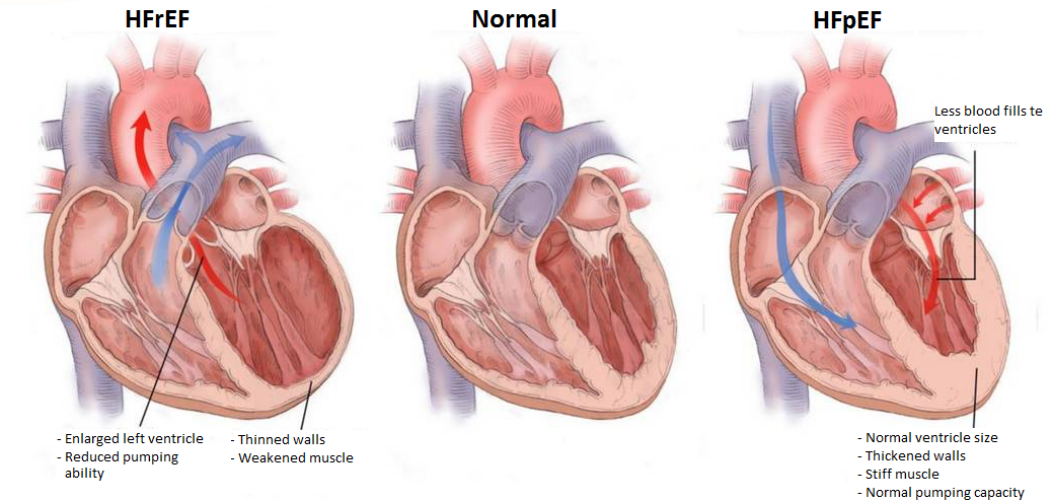

Fig. 1: Anatomy of a normal heart (middle), a heart in case of heart failure with reduced ejection fraction (left) and a heart in case of heart failure with preserved ejection fraction (right), adapted from: [8].

The measurement of the left ventricular ejection fraction (LVEF), which indicates the amount of pumped blood each contraction, is used to describe the wide range of patients with HF. Patients with a normal LVEF (considered as $\geq$ 50 %) are classified as heart failure with preserved ejection fraction (HFpEF), while patients with reduced LVEF (considered as $<$ 40%) are classified as heart failure with reduced ejection fraction (HFrEF). The grey area of patients with an LVEF in the range of 40-49% is classified as heart failure with mid-range ejection fraction (HFmrEF). Figure 1 shows a schematic demonstration of the anatomical situation for a normal heart, a heart in case of HFrEF and a heart in case of HFpEF. Physiological changes in HF are mentioned in Appendix A, Section 6.3.

1.3 Current treatments of heart failure

The purpose of treatment in patients with HF is to improve their clinical condition, quality of life and functional capacity, prevent hospital admission and reduce mortality. A pharmacological treatment with diuretics, angiotensin-converting-enzyme (ACE) inhibitors and beta-blockers is recommended for treatment of patients with HFrEF [5]. In patients with a conduction disorder, for example a left bundle branch block, cardiac resynchronisation therapy (CRT) can improve cardiac performance and symptoms. CRT improves refilling and contraction pattern of both ventricles, by using a right atrial pacing electrode and a right and left ventricle pacing electrode. The indication for CRT is limited to patients which are symptomatically and medically treated for heart failure and have inter- or intraventricular conduction disorders and a reduced EJECTION FRACTION (EF) [5]. However, 30 – 40% of the patients who are treated with CRT remain non-responders [9].

Another more invasive treatment option is a left ventricular remodeling operation or in case of end-stage heart failure, the implantation of a left ventricular assist device (LVAD) as a bridge to heart transplantation. A big limitation of a LVAD is the necessity of anticoagulant therapy, because of the thrombogenic surfaces such as mechanical valves which are exposed

to blood. However, due to limitations of a heart transplantation, such as a shortage of donors, rejection and infection, LVADs are frequently implanted as a bridge to transplantation or even as a destination therapy [10]. Appendix A (Subsection 6.3.5) provides a more detailed description of above-mentioned treatments. Due to limitations of LVADs, heart transplantation and CRT, it is desirable to develop a new resynchronisation therapy in which all HFrEF patients are eligible for treatment.

1.4 Proposed solution

A proposed solution is to develop a device which is able to provide an additional contraction, at one or multiple places of the heart. The part of the device which should provide this additional contraction of the heart, should be able to change its form under the influence of an electrical pulse. After maximal deformation, the material should return to its original shape, which makes it possible to deform again after a new electrical pulse. Possibly a smart material, such as an shape memory alloy (SMA) or an shape memory polymer (SMP) is suitable for this purpose.

SMAs are metallic alloys with two, three or four components, with special compositions. A well-known SMA is the nickel-titanium (NiTi)-based SMA, also called NiTi-alloy or Nitinol. SMAs display two distinct crystal phases: the austenite phase at high temperature and the martensite phase at low temperature. During the martensite phase, the SMA can be easily deformed. When an SMA is heated during the martensite phase, the SMA is reverted into austenite phase in which the original austenitic structure is restored and is responsible for its "shape memory" [11]. The change between the different phases is shown in Figure 2 [12].

SMPs have, like other shape-memory materials, a shape-memory effect. Production of an SMP starts with forming the polymer in its permanent shape [13]. Thereafter, the polymer is deformed and attached into a temporary shape. From this temporary shape, the polymer can recover to its permanent shape after activation by an external stimulus. Additional information about SMAs and SMPs can be found in Appendix B, Section 7.1.

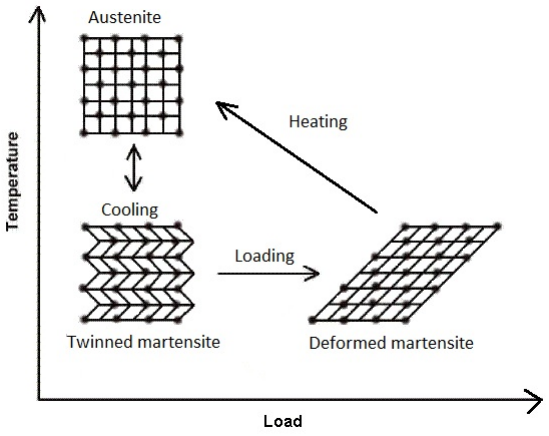

Fig. 2: Shape memory effect of shape memory alloys (adapted from: [12]).

This study investigates whether a smart material driven by an electrical pulse (preferably a pacemaker), is able to support and strengthen the pump function of the heart, and therefore serve as a possibly new resynchronisation therapy in HFrEF patients. The main goal of this study is to investigate if it is possible to reach an EF of 5% in a static heart model, because treatment which causes an increase in EF with 5% can already cause clinical improvement in HF symptoms and therefore quality of life [14–16].

The sub-goals of this study are:

- To determine optimal designs of shape memory alloys in a static in vitro model.
- To determine optimal power supply of shape memory alloys.
- To determine the temperature development and the effect of insulation of shape memory alloys.

The hypothesis is that an SMA with a larger diameter which covers a large part of the ventilation balloon and creates forces in multiple directions will give the best results. Furthermore, the hypothesis is that a higher duty cycle and insulation will cause a faster heat up of the SMA and that too fast consecutive activation of SMA will oppose the results.

2 Methods

2.1 Materials and test setup

The contractile ability of NiTi-wires was examined on a static model with a paediatric ventilation balloon (Laerdal Benelux bv, Amersfoort, The Netherlands) as a dilated heart model, see Figure 3. The ventilation balloon is made of silicone rubber, which has the advantage to preserve elasticity and therefore a good representative of the heart. The volume of the flexible part of the ventilation balloon is 475 mL. The ventilation balloon was connected to a clear tube to monitor the outflow after activation of the shape memory alloy (SMA). Silicone vascular ties and Velcro straps were used to fasten the SMA around the balloon. Furthermore, SMA-wires were connected to small power cables by cable shoe connectors and attached to screw terminals for a tight fixation.

Fig. 3: Test setup with a ventilation balloon as a heart model.

2.2 Shape memory alloys

The applied SMAs in this study are the Flexinol® actuator wires (Dynalloy Inc., Irvine, California, United States), made of nickel-titanium (NiTi). NiTi-wires have a diameter of 150 μm, 250 μm and 380 μm, with a transformation temperature of 70 °C [17]. The density of Flexinol® is 6.45 g/cm^3, its specific heat 0.2 cal/g°C and it has a thermal conductivity of 0.18 W/cm°C.

2.3 Design

Different ways of SMA application were considered, which is described in Appendix C, Chapter 8. Designs which were finally investigated around a heart model are a spiral, band, cross and oblique shape of the SMA, which are shown in Figure 4. A list of requirements for application of SMA in case of HF can be found in Appendix C, Chapter 8. The requirements which are considered to be most important are:

- Allow rotation of left ventricle apex during systole and not oppose its function during isovolumic relaxation and early period of diastole [18].
- Should be able to displace additional volume.

- Should be biocompatible.
- Should have a durability of approximately five years.

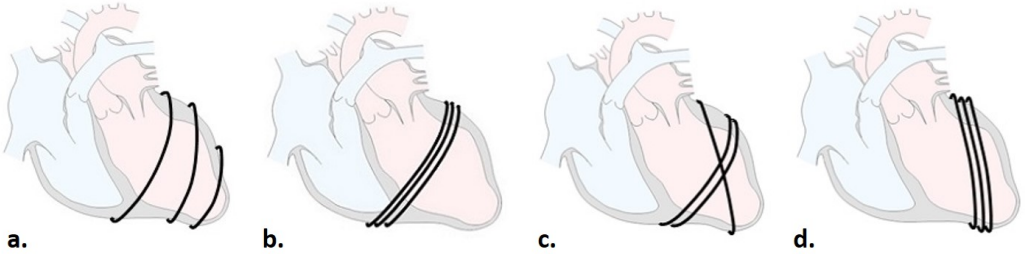

Fig. 4: Heart supported by different configurations of SMA. a) Spiral. b) Band. c) Cross. d) Oblique.

2.4 Pulse width modulation technique

Activation of SMAs was performed by pulse width modulation (PWM) technique with a pulse generator. Figure 5 shows a schematic representation of the experimental setup with the power supply. The SMAs around the heart model were activated by an electrical pulse from a pulse generator and a power supply. The pulse generator uses PWM to restrict heating and to better control electrical activation of the SMA. The pulse generator consist of three variables: frequency, duty cycle and intervals between SMA activating pulses. Variables of the pulse generator (pulse frequency, activating pulse intervals and duty cycle) influence SMA activation and thereby the amount of displaced volume. Pulse frequencies of 50, 60, 70, 80, and 90/min, activated pulse intervals from 1 to 5 and duty cycles of 20 to 80% were examined. Additional information about PWM technique can be found in Appendix B, Subsection 7.2.1.

2.5 Experiments

2.5.1 Configurations for volume displacement of SMA

Displaced water as a result of SMAs contraction was recorded with a compact camera and analysed by using Kinovea 0.8.15 software. The volume level in the tube was tracked with this software as a function of time. To determine the optimal configuration for volume displacement, graphs were made for different configurations of SMA. Designs were reviewed on achieved volume displacement based on these graphs.

2.5.2 Influence of SMA diameter on volume displacement

The diameter of an SMA has influence on its cooling time and the amount of created force. To consider optimal interaction between power supply and created force, SMAs with different diameters (150 μm, 250 μm and 380 μm) were analysed. The results of a band shape with one to five windings was presented in one figure, by plotting mean volume displacement of the last four pulses against the number of windings.

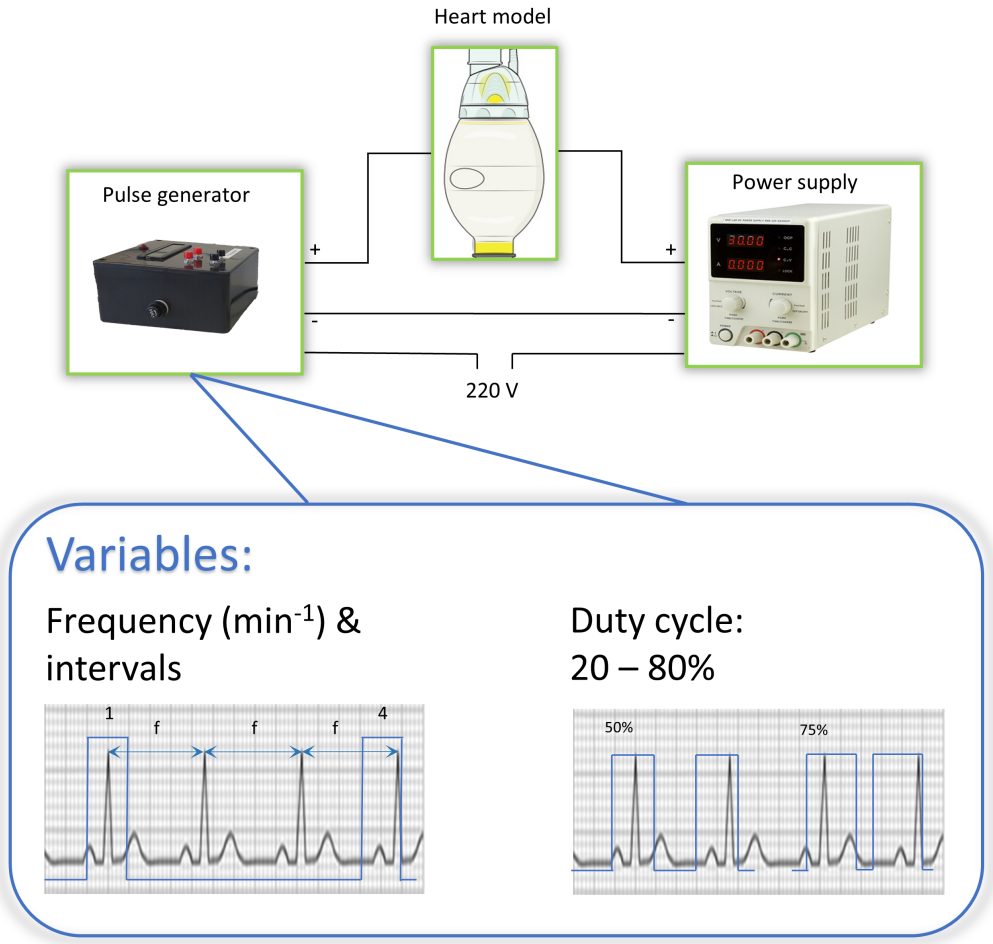

Fig. 5: Schematic representation of test setup. Pulse generator, which activates the SMAs around the heart model has three variables: the frequency, duty cycle and intervals.

2.5.3 Temperature development and insulation

To determine temperature development and role of insulation, temperature progression was monitored with a thermal camera (FLIR C2, FLIR Systems, Wilsonville, USA). Specifications of this thermal imaging camera are summarised in Table 2. Temperature signals of these thermal images were filtered with a High-pass Butterworth filter in Matlab R2016b (MathWorks, Natick, USA) to filter linear drift caused by the thermal camera.

Table 2: Specifications of Flir C2 Thermal camera

Specification	Value
IR Sensor	80 x 60 (4800 measurement pixels)
Thermal Sensitivity	< 0.10 °C
Object themperature range	-10 °C to 150 °C
Accuracy	± 2°C or 2%

2.5.4 Pressure build-up

An external pressure sensor was fabricated to measure pressure build-up in the ventilation balloon during SMA activation. A balloon which is normally used during transcatheter aortic valve implantation (TAVI), was placed in the ventilation balloon and connected to an intravenous blood pressure sensor (501669001, Merit OEM, Maastricht), which in turn was connected to a microcontroller (Arduino Uno, Arduino) to interpret pressure values on a laptop. Raw data was filtered with a High-pass Butterworth filter and a Moving Average filter. More detailed information about this pressure sensor can be found in Appendix B, Subsection 7.2.3.

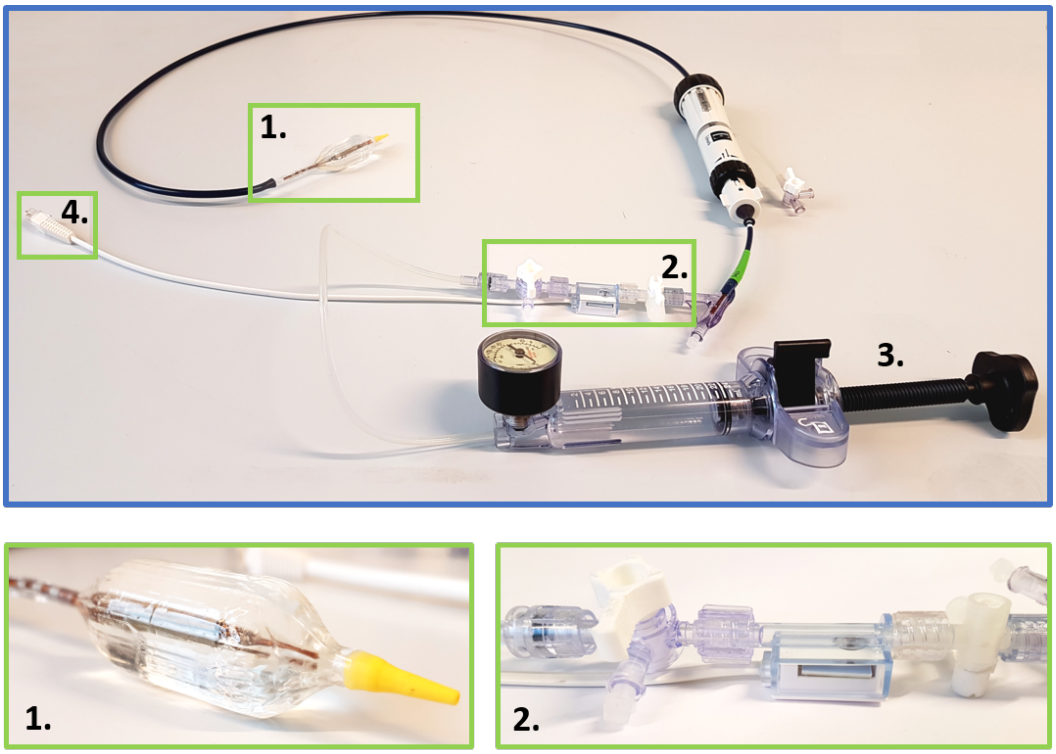

Fig. 6: Pressure sensor. 1. Inflatable TAVI balloon placed in ventilation balloon. 2. External pressure sensor. 3. Hand pump with pressure gauge to fill TAVI-balloon with water. 4. Connection to pressure sensor and microcontroller.

2.5.5 Statistics

Results were considered statistically significant at the 5% level. Resulting graphs of the experiments were made with GraphPad Prism 5 (Graphpad Software, Inc., San Diego, CA). Furthermore, GraphPad Prism 5 was used to perform a one-way ANOVA and a Tukey post hoc test for the experiments with different SMA configurations and activation frequencies, and a repeated ANOVA with a Tukey post hoc test for the experiment with different pulse intervals. And as last, a linear regression analysis for different diameters of SMA. Results are reported as mean $\pm$ SD.

3 Results

3.1 Configurations for volume displacement of SMAs

Figure 7 shows volume displacement of four different configurations of the SMA. A configuration where the SMA was formed in a spiral shape around the heart model caused the highest displaced volume (6.2 mL). SMAs which were placed in a band or cross shape, achieved a displaced volume which was close to the spiral shape, with a value of 5.7 and 5.5 mL, respectively. A configuration which achieved a much lower value, is the oblique shape with a maximal displaced volume of 3.4 mL. There was a statistically significant difference between configurations, as determined by one-way ANOVA ($F(3,24) = 34.83$, $p < 0.0001$). A Tukey post hoc test revealed that volume displacement was statistically significantly lower for the oblique configuration (2.9 mL $\pm$ 0.3, $p < 0.05$), compared to the band (4.8 mL $\pm$ 0.6, $p < 0.05$), spiral (5.0 mL $\pm$ 0.4, $p < 0.05$) and cross shape (4.6 mL $\pm$ 0.3, $p < 0.05$). There was no statistically significant difference between band and spiral, band and cross and between spiral and cross shape.

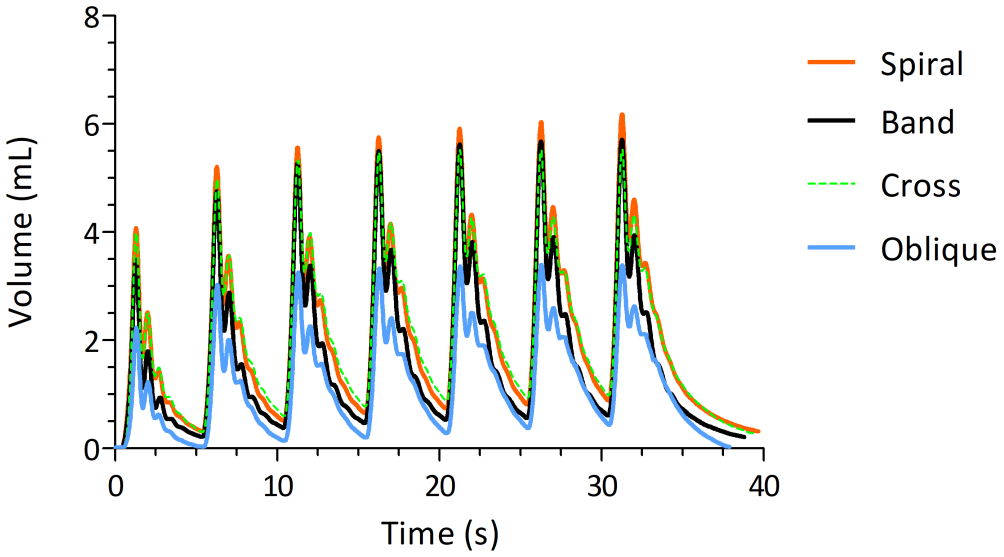

Fig. 7: Different configurations of SMA. Volume displacement was statistically significant lower for the oblique configuration, compared to other configurations.

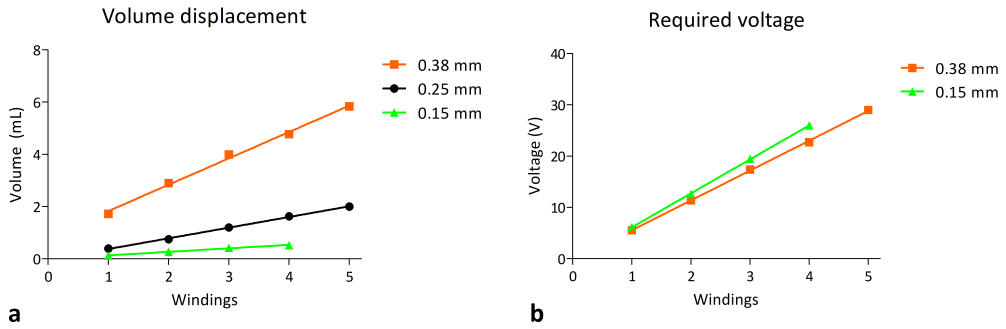

Fig. 8: Diameter influence. a) Volume displacement for increasing number of NiTi-wires with diameters of 0.15 mm, 0.25 mm and 0.38 mm. b) Amount of SMA windings and required voltage for SMAs of 0.15 mm and 0.38 mm. Individual data point are connected with a linear regression line ($r^2 = 0.99$) in both graphs.

3.2 Influence of SMA diameter

Figure 8 shows the influence of the SMAs diameter on volume displacement and required power supply. Maximal volume displacement of three different diameters (0.15 mm, 0.25 mm and 0.38 mm) of SMA are presented for one to five individual horizontal SMA-wires. Figure 8a shows that the maximal volume displacement increases almost perfectly linearly with increasing number of windings around the heart model: $r^2 = 0.99$. The same applies to the required voltages, as can be seen in Figure 8b. Required voltage of 0.25 mm SMA-wire was not plotted due to used parallel circuit instead of a serial circuit. There was a statistically significant difference between different diameters of SMA, as determined by one-way ANOVA ($F(2,11) = 14.32$, $p < 0.001$). A Tukey post hoc test revealed that volume displacement was statistically significantly higher for the 0.38 mm SMA-wire (3.8 mL $\pm$ 1.6, $p < 0.05$), compared to the 0.25 mm SMA-wire (1.2 mL $\pm$ 0.6, $p < 0.05$) and the 0.15 mm SMA-wire (0.3 mL $\pm$ 0.2, $p < 0.05$). There was no statistically significant difference between the 0.25 and 0.15 mm SMA-wire.

3.3 Variables of pulse width modulation technique

3.3.1 Pulse frequency

Adapting the pulse frequency resulted in a different activation of SMA. Volume displacement of five different frequencies (50, 60, 70, 80 and 90 min^{-1}) are presented in Figure 9.

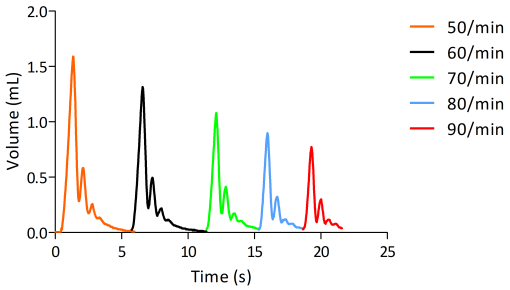

Fig. 9: Pulse frequency. Volume displacement of every third pulse at different frequencies.

Figures from other frequencies can be found in Appendix E, Chapter 10. Duty cycle and interval rate were kept constant at respectively 75% and 5. As can be seen from this figure, the maximal displaced volume decreases with a higher pulse frequency. The complete overview of the influence of pulse frequency on volume displacement, which is presented in Appendix E (Figure 67), shows that volume displacement reaches a constant volume after three pulses, regardless of the used pulse frequency. There was a statistically significant difference between different pulse frequencies as determined by one-way ANOVA ($F(4,25) = 399.4$, $p < 0.0001$). A Tukey post hoc test revealed that the volume displacement for a frequency of 50% was statistically significantly higher (1.6 mL $\pm$0.04, $p < 0.05$), compared to other frequencies. The same applies to the other higher frequencies.

3.3.2 Duty cycle

Another important variable of the pulse generator, that influences the activation of SMAs, is the duty cycle. Figure 10 shows the mean volume displacement for duty cycles from 20 to 80%. As can be seen from this figure, the displaced volume increases with higher duty cycles. Influence of the height of current on the rate of volume rise, the flow, is presented in Figure 11. Maximal, mean and minimal flow out of the first five pulses are shown with an orange, black and green line, respectively.

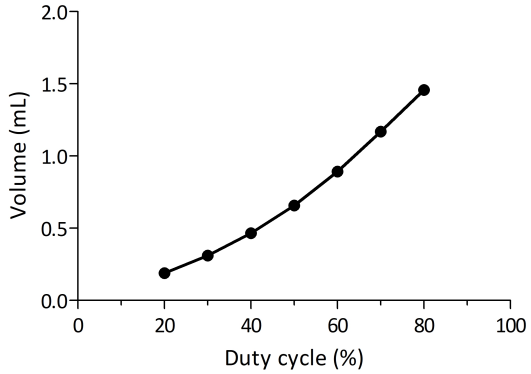

Fig. 10: Variation of duty cycle. Each dot represents the mean volume displacement of the last three pulses of the specific duty cycle. SEM for each dot was so low that it was not plotted. Individual graphs can be found in Figure 66 in Appendix E.

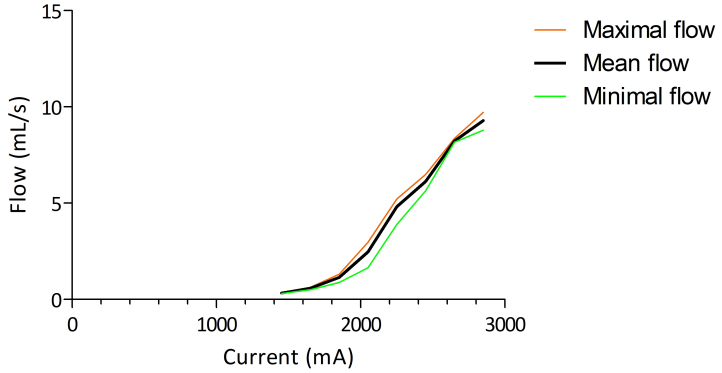

Fig. 11: Influence of current on flow. Maximal (orange), mean (black) and minimal (green) flow are plotted against applied current.

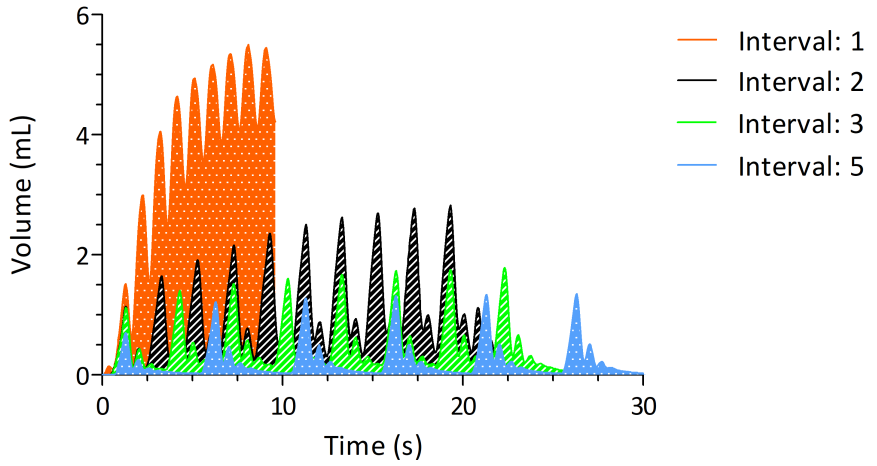

Fig. 12: Pulse interval. Volume displacement for different number of intervals. Volume displacement changes drastically when every heart beat (interval of 1) is supported, compared to other pulse intervals.

3.3.3 Pulse intervals

Results of adapting the pulse interval variable are presented in Figure 12. As can be seen from this figure, the graph of the volume displacement changed drastically in case of an interval of one, in which the device should support every heart beat at a frequency of 60/min. A repeated measures ANOVA determined that maximum volume displacement differed statistically significantly between time points ($F(4,20)=13.84$, $P < 0.0001$). Post hoc tests using the Tukey correction revealed that the increase in absolute volume displacement over time was statistically significant different for an interval of 1 (2.0 mL $\pm$ 0.4) and the intervals 3 (1.4 mL $\pm$ 0.2, $p < 0.01$), 4 (1.3 mL $\pm$ 0.1, $p < 0.001$) and 5 (1.2 mL $\pm$ 0.2, $p < 0.001$). Furthermore, increase in volume displacement was also statistically significantly different between an interval of 2 (1.7 mL $\pm$ 0.4, $P < 0.05$) and intervals 4 and 5. Differences between the other mutual intervals were not statistically significant.

3.4 Temperature

The transformation temperature of the used SMA wires is 70°C, which was reached by applying an electrical current.

3.4.1 Temperature development

Figure 13 shows the temperature change of the SMA wire (0.25mm) during multiple activation cycles. From this graph we can see that maximal temperature is reached after four activation cycles. After this fourth cycle, temperature rises and decreases constantly between two imaginary parallel and horizontal lines.

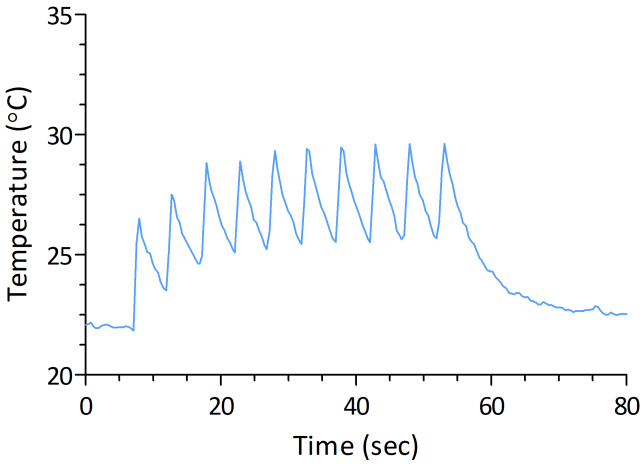

Fig. 13: Temperature development of Flexinol-wire (0.25mm), as determined by a thermal camera.

3.4.2 Insulation

For future implantation of SMAs in the human body, insulation is needed. This subsection describes the effect of insulation of the SMA-wire. Figure 14 shows a 0.38 mm Flexinol®-wire with two small pieces of silicone tubing, which insulated the wire. The left picture shows the schematic representation in which the small pieces of insulation are indicated with arrows. The right picture shows the thermal image of the partial insulated SMA-wire. As can be seen, the two small pieces of wires are insulated and retain the heat through the silicone tubes.

The measured temperatures of SMA-wires with and without insulation, after installation around the ventilation balloon, are shown in Figure 15. The black line displays the wires without insulation and the orange line displays the case in which the wires were fully insulated with a silicone tube. As can be seen in this figure, a higher temperature was

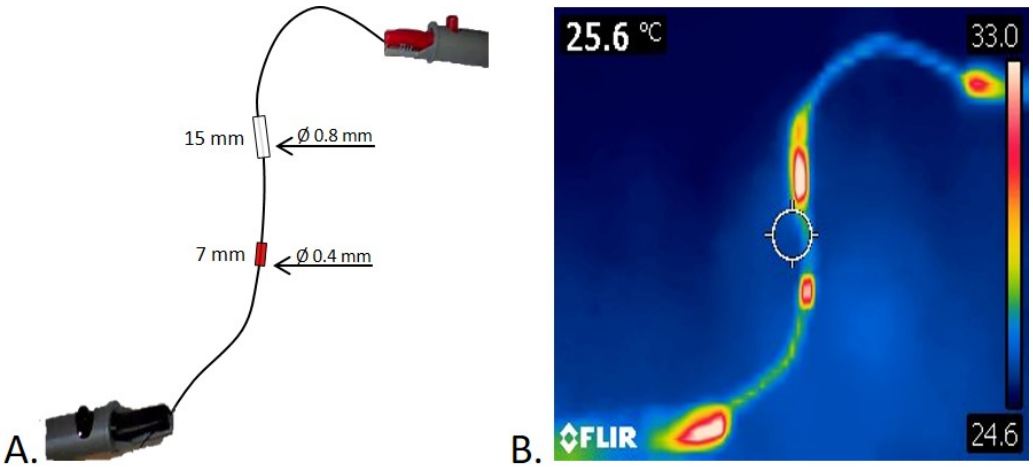

Fig. 14: Insulation of SMA-wire. A) Schematic representation of an SMA with two small pieces of silicone insulators. Size and diameter are shown in figure. B) Corresponding thermal image.

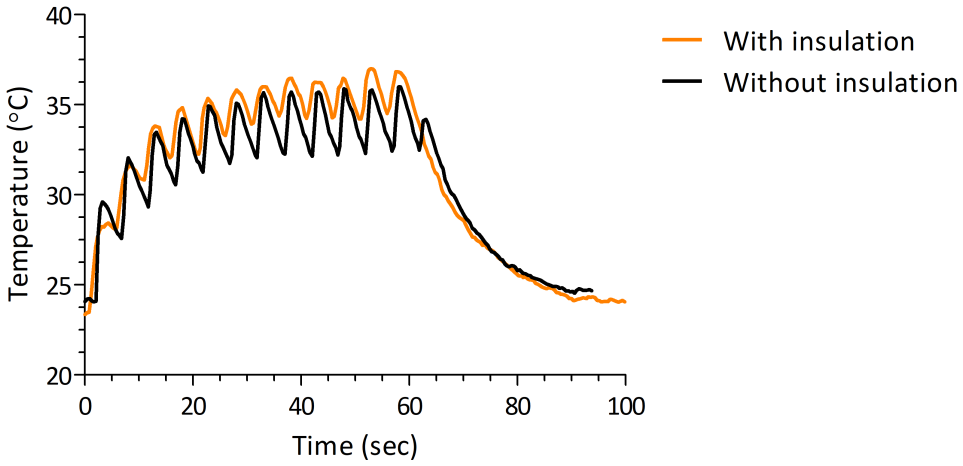

Fig. 15: Temperature of SMA-wire of 0.38 mm, with insulation (orange line) and SMA-wire without insulation (black line). Each rise in temperature corresponds to an activation pulse of the pulse generator.

reached in case of insulation, compared to the wires without insulation. Furthermore, temperature for insulated wires decreased not as far as for wires without insulation.

The volume displacement in case of an SMA-wire (0.38mm) with and without insulation is shown in Figure 16. It shows that the volume displacement in time, shows the same course for both cases, in which the volume displacement increases for the first six pulses and thereafter stabilises. However, the maximal volume displacement which is reached, is in case of insulation lower compared to the situation without insulation.

Figure 17 shows the results of a longer measurement of two individual wires of SMA, one with a silicone tube and one without insulation. We see that temperature fluctuates constantly, for both SMA with insulation (shown in orange) and SMA without insulation

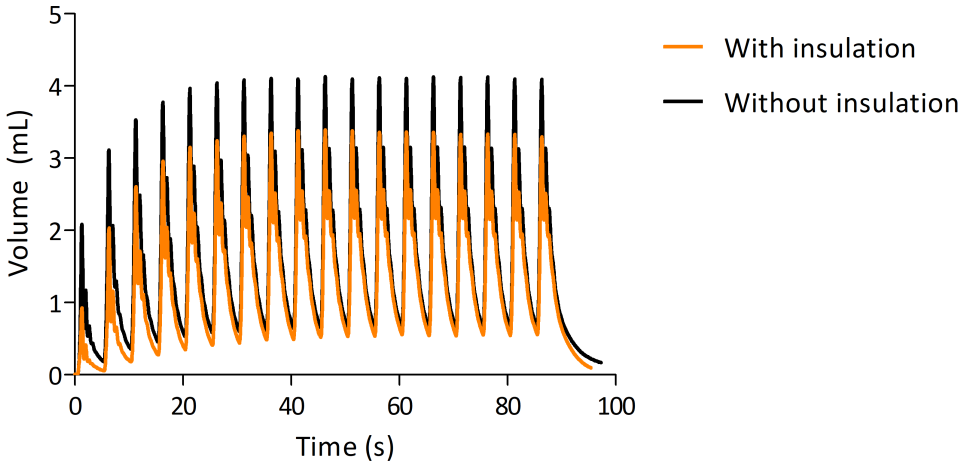

Fig. 16: Volume displacement of 0.38 mm SMA-wire, without insulation (black line) and with insulation (orange line).

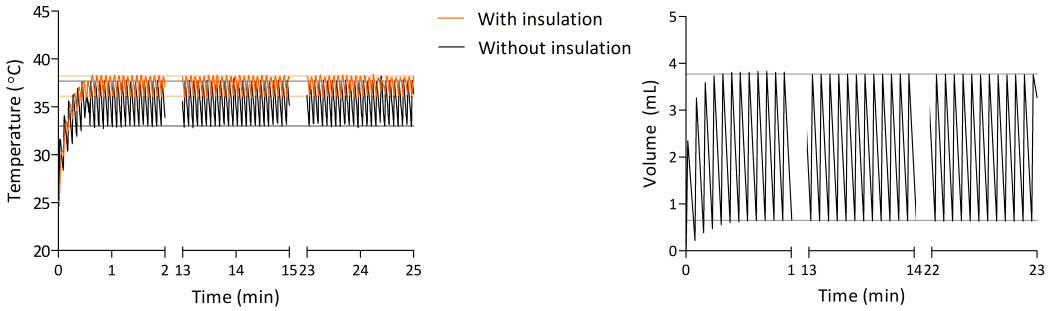

Fig. 17: Prolonged measurement of two windings of 0.38 mm SMA-wire, one with and one without insulation. Left figure shows temperature fluctuations of the individual SMA-wires, with reference lines of the corresponding mean of highest and lowest measured temperature. Right figure shows the corresponding volume displacement of the SMA-wires, also with reference lines which indicate the mean of the minimal and maximal measured values.

(shown in black), even after twenty minutes. The same applies to the corresponding volume displacement of the two SMA-wires, which also remains constant after a while.

3.5 Pressure build-up

Results of measured pressure with the pressure sensor are presented in Figure 18. The left graph shows the volume displacement (in cm) within the tube, while the right figure shows the pressure within the ventilation balloon (tube was removed) over time. With Equation 3.1 pressure difference (ΔP) can be calculated, in which ρ is the density of the liquid (in [kg/m^3]), g is the gravitational acceleration (in [m/s^2]) and h the height difference of the liquid with respect to the initial situation. With this equation and the left graph of Figure 18 a pressure of 7.6 mmHg was calculated for the fifth pulse, in case of the initial setup. With the pressure sensor, a pressure difference of 7.3 mmHg was measured for the fifth pulse.

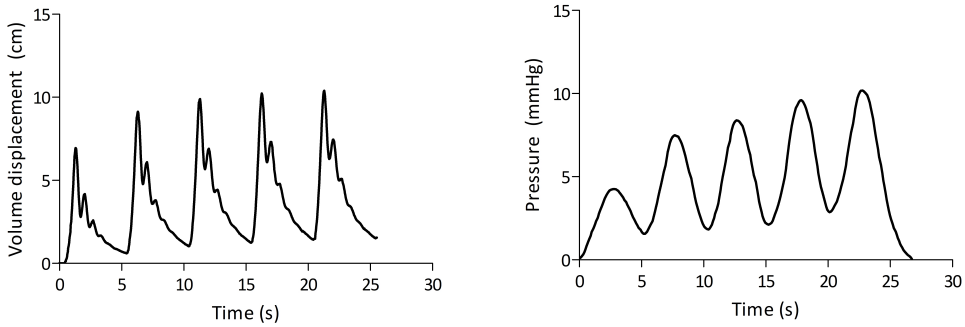

Fig. 18: Pressure measurement. On the left a graph based on the initial test setup and on the right a graph of the measurement with an external pressure sensor.

$$\Delta P = \rho \cdot g \cdot h \tag{3.1}$$

The maximal displaced volume in cm, for recommended current supply (2.25A), was 13.95 cm for a band shape which consisted of five windings. With Equation 3.1 it can be calculated that this volume displacement corresponds to a pressure of 10.3 mmHg. A measurement with much higher current (2.850 A) and rings to distribute forces upon the balloon, resulted in a volume displacement of 16.4 mL (32.8 cm in case of 8 mm tube), which corresponds to a pressure of 24.1 mmHg.

4 Discussion

4.1 SMA configurations

The results of the experiment with different designs of SMA showed that the spiral shape causes the highest volume displacement for the used static heart model. Volume displacement achieved by a band and a cross shape where close to the spiral shape, while the volume displacement of the oblique shape was noticeably lower. The results of this study match those observed in earlier studies with the same heart model [19, 20]. However, measured volume displacements were quantified and turned out to be higher in this study. From the statistical analysis it can be concluded that an oblique shape is not an effective design, but that the other three designs are still an option because the volume displacement did not differ significantly between these groups. The finding that a design which resembles the myocardial tissue results in higher volume displacement is consistent with those of Shiraishi et al. [21], who investigated three different designs that are more or less the same as the used designs in this study [1]. This suggest that it is important to approach the anatomical structure of myocardial tissue.

4.2 Diameter of SMA

The results in Section 3.2 showed that the volume displacement and the required voltage increases linearly with the used number of SMA-wires, for all three examined diameters. This suggest that it is possible to predict the number of needed SMA-wires (in the band shape design), for a desired amount of volume displacement, and which voltage is probably needed.

The corresponding equation for the relation between number of windings and displaced volume for a 0.38 mm NiTi-wire was: $V = 1.010 \cdot n + 0.8189$, in which V is the displaced volume (mL) and n the number of windings. With this equation it can be calculated that for reaching a EF of 5% (=23.75 mL), 23 windings will be needed. However, it is likely that after a certain number of windings, volume displacement will not further increase. On the other hand, the calculations may be an underestimation because of the high amount of volume in the balloon, which will be explained later.

[1] Note that the used terms for the different designs are confusing, compared to the terms used in this study. The mentioned oblique type of Shiraishi et al. looks like the spiral/cross shape instead of the oblique design of our study

4.3 Pulse width modulation

Figure 8 showed the influence of the duty cycle from the pulse generator on the corresponding volume displacement, caused by SMA activation. The decreasing volume displacement, at an increasing frequency is caused by the shorter pulse duration, see Subsection 7.2.1. Statistical analysis showed that volume displacement was statistically different in all measured frequencies. The results of another variable of the pulse generator, the duty cycle, were shown in Figure 10. A higher duty cycle means that the signal is on for a longer period of time.

The influence of number of pulse intervals, was shown in Figure 12. As mentioned in Subsection 3.3.3, a pulse interval of one showed a completely different volume profile, compared to the other pulse intervals. The fact that the volume displacement did not decrease to zero before the consecutive pulse arises, suggest that the SMA has not enough time to cool down between consecutive pulses. According to the statistical analysis it can be concluded that activation of SMA with a pulse interval of 1 or 2 should be avoided and pulse intervals of 3, 4 or 5 give better results in this heart model.

4.4 Temperature

Transformation temperature is an important factor for implementation of SMAs in medical devices. This section will therefore discuss the temperature results of this study and results of other studies with SMAs.

4.4.1 Temperature development

Results of temperature measurements in this study showed that temperature changes, as a result of activation of the SMA-wire by electric current, can be monitored with a thermal imaging camera. Unfortunately, the measured absolute temperature of the SMA-wire seems not to be realistic, because activation temperature of the used SMA-wires is 70 °C, while the measured maximal temperature of the 0.25 mm Flexinol wire was 30 °C. This inaccuracy is mainly caused by the quality of the thermal image camera, which will be further explained in Appendix B, Subsection 7.2.2.

The heating rate of an SMA-wire can be increased by passing a larger current through it [22]. However, an excessive electrical current can overheat the SMA and thereby causing stress fatigue and a decrease in the number of transformation cycles. Figure 11 showed that indeed the SMA-wire was activated faster (higher flow) in case of higher current. The hysteresis shape of this graph, which can be seen even more clearly in Figure 70 in which maximal volume is plotted against the applied current, shows the range of current which lie in the linear range. Chance of overheating the SMA-wires with currents which lie in this linear range is very low. Conversely, applying currents which lie in the high plateau phase will not result in much higher values of volume displacement (and flow), and the chance of overheating and fatigue of the SMA-wire will be higher in this range. It is therefore recommended to apply current within the linear range of the curve.

4.4.2 Insulation

Although it turned out that measurements of absolute temperatures was not accurate, Figure 14 showed that it is possible to insulate the SMA-wire with silicone tubing, because the same colour pattern was seen at the parts with silicone tubing as at the insulated clamps that hold the SMA-wire. Furthermore, the thermal images of this SMA-wire with silicone tubes showed that maximal observed temperatures lasted longer at the parts with silicone tubing, which suggest that the silicone parts caused that the SMA-wire cooled down more slowly at these specific spots and heat was kept within the silicone tube.

This observation was also observed in Figure 15, in which the temperature of the SMA-wire with insulation fluctuates within a smaller range compared to the SMA-wire without insulation. The maximal absolute temperature values of the insulated wires were higher than for the wires without insulation. Despite it is difficult to draw conclusions from the measured absolute temperatures, a possible reasons for this difference in maximal temperature can be mentioned. It is for example possible that due to the retained heat, the thermal camera has more time to determine the temperature, causing a higher temperature in case of an insulated SMA-wire.

The measured maximal volume displacement was higher for SMA-wires without insulation than for the insulated SMA-wires (see Figure 16). This finding is consistent with those of Kalogerakos et al. [23], who also observed a higher output in case of SMA-wires without insulation. The reason for the lower output, in case of insulation, could be that the relaxation time of the wire is delayed or due to the insulation tubes itself, which are maybe not flexible enough or their diameter is too big and causes an inefficient SMA contraction.

4.4.3 Stability

As observed in Figure 17, volume displacement and temperature fluctuations remained stable during a long-term measurement. This shows that during this measurement, there was no fatigue of the SMA-wires, and outcome (volume displacement) remained stable during the whole measurement. The results of a long-term measurement in which one SMA-wire was disconnected from the screw terminal and therefore caused a decrease in volume and temperature, are shown in Appendix E (Figure 71).

4.5 Pressure build-up

The measured pressure with the pressure sensor (7.3 mmHg) was quite similar to the determined pressure from the displaced volume by using the initial setup (7.6 mmHg). Furthermore, the graph of the measured pressure also showed an increase in peak height in consecutive pulses, which was also observed in the graph in which pressure was determined from the volume displacement. This finding confirms that it was possible to measure the pressure within the ventilation balloon with a self-made external pressure sensor. However, it should be noted that the external pressure sensor had a resolution of 1.63 mmHg, which makes a possible error in measurements of low pressures quite big.

Unfortunately, it was not possible to compare the measured pressures with other studies, due to a different setup.

4.6 Applicability of the device

Application of SMA in patients with heart failure has some challenges, which will be mentioned below.

4.6.1 Safety

A safe application of SMAs in patients is crucial, especially in case of activation with an electrical current. Besides protection of damage through heat of the SMA, insulation should also protect surrounding tissue for the required current to activate SMA-wires. Electric shocks can immediately affect cardiac cell function, because they are electrically excitable. An exposure to low-voltage can result in ventricular fibrillation and an exposure to high voltage/current even in asystole [24]. Ventricular fibrillation can occur in 5 s and 0.1 s, when there is exposure of 120 mA or 1.2 A, respectively [25]. This shows that it is extremely important to insulate the wires, not only for heat but especially for the current itself. Further research is required to establish if silicone tubing is an effective heat and current insulator.

4.6.2 Power supply

An overview of several existing LVADs and their power consumptions is described in Appendix B, Section 7.3. The power consumption of these LVADs lie roughly between 7 and 10 Watts. By way of comparison, power consumption of regular pacemakers are in order of micro Watts.

For the best design out of Figure 7 (spiral shape), an energy consumption of 5.5 watt-hours was needed. The used voltage of this measurement was 16.3 V and for every pulse, a current of 2.25 A was given for 750 msec. The energy is therefore: E = 16.3 V x 2.25 A x 0.75 sec = 27.51 J. In 1 hour, the device would contract 720 times (12 contractions/min x 60 min); therefore, the hourly energy consumption is 19804 J (27.51 J x 720 contractions) which is equal to 5.5 watt-hours.

Applying higher currents (and force distribution) to the SMA made it possible to increase stroke volume and thus EF. The energy consumption for the highest EF (3.5 %) in this study was 11.4 watt-hours. The voltage was 25 V and for every pulse, a current of 2.850 A for 0.960 msec was used. The energy was therefore: E = 25 V x 2.85 A x 0.96 sec = 68.4 J. In 1 hour, the device would contract 600 times (10 contractions/min x 60 min); therefore, the hourly energy consumption is 41040 J (68.4 J x 600 contractions) which is equal to 11.4 watt-hours.

Most regular pacemakers have a power supply of 2.5, 5 or 7.5 Volt [26]. Furthermore, most pacemaker batteries have a capacity between 1 and 2 Ah, while an implantable cardioverter defibrillator (ICD) has a somewhat higher capacity between 1.5 and 2.5 Ah [27]. Activating

SMA-wires of 0.38 mm with a current of 2.25 A (or higher), is therefore unfortunately not possible with regular pacemaker/ICD batteries at this moment. However, the hourly energy consumption of SMA activation in this study (5.5 and 11.4 watt-hour) is lower than the hourly energy consumption of a LVAD which is 23.6 watt-hour in case of the HeartMate II (see Appendix B, Section 7.3).

In this study measurements were performed at room temperature. According to Hassoulas et al. less energy is required when SMA is activated at body temperature [28]. In their study, a duty cycle of 50% produced a bigger strain in case of a higher ambient temperature. This means that it is expected that a reduction in duty cycle can produce the same volume displacement, when measurement are performed in an ambient temperature which is close to body temperature. In turn, this will cause a longer battery life.

4.6.3 Fixation

Fixation of the SMA-wires is extremely important to optimise the resulting force, caused by SMA contraction, on the ventricles. During experiments, it was found that fixation of SMA-wires is not that easy. Due to the created forces during activation of SMA, wires were occasionally released from the screw terminal. This interrupted the electric circuit, which is unwanted when it will be implanted in a patient. Besides fixation of the SMA-wires with the electrical wire, a good fixation of the (insulated) SMA-wires to the heart wall is very important to prevent dead space between SMA-wires and pericardium. The best way of fixation should be investigated, but maybe trabeculae-like elements from the insulated SMA-wires to the heart wall or biocompatible glue will be an option.

4.7 Limitations of the study

Although this research has been carefully prepared and implemented, there were still some limitations and shortcomings. First of all, the used ventilation balloon as a heart model caused some limitations. The ventilation balloon consisted for example of only one chamber and one output. It was therefore not possible to determine the influence of contraction of SMA-wires on the distinctive left and right ventricle. Although the results of this study gives insight into the possibility of NiTi-wires to displace volume in a static heart model, the amount of displaced volume will probably be different in in vivo experiments. In this case, the left ventricle will not be fully surrounded with SMA-wires, but will be partly compressed indirectly by the compression of the right ventricle. Furthermore, end-diastolic volume will be smaller than volume of this model (475 mL), which will probably result in a higher stroke volume and ejection fraction, according to Laplace's law. This law states that the efficiency of ventricular ejection decreases when radius of the ventricle increases, because a greater wall tension is needed to maintain the pressure for ejection of blood [29]. Secondly, even though the silicone rubber of the ventilation balloon has the advantage that it preserves elasticity, it has some material characteristics which makes it difficult to simulate a human heart. The elasticity of the silicone ventilation balloon caused for example multiple peaks (during the back flow to the balloon), while this will be absent in a beating heart.

Furthermore, the resolution of the thermal camera was not high enough to measure absolute temperatures of the thin SMA-wires. Although it was possible to determine temperature changes with the thermal camera, exact temperature measurements are needed to find out if the contractions of the SMA-wires take place in the linear range of its temperature-strain curve.

4.8 Recommendations

This study proved that it was possible to displace volume with SMA-wires in a static heart model. The expectation is that in case of a beating heart, the work of SMA-wires will contribute to a higher pump action and therefore to a higher volume ejection. To confirm this hypothesis it is recommended to repeat the measurements in a dynamic heart model, which can simulate the beating heart and therefore makes it possible to investigate if the contribution of SMA-wires is indeed higher in a dynamic model compared to the static heart model. Measurements in a ventricle which in size is comparable to a dilated ventricle, and therefore smaller than the amount of volume in the model of this study, should show if EF is indeed higher in that case. A dynamic heart model in which also the preload and afterload can be adapted will make it possible to mimic a realistic situation of a beating heart. Furthermore, adding an internal pressure sensor and flow sensor will provide a quicker analysis of the measurements.

In Eindhoven, researchers developed a dynamic heart model with a pig heart, which creates a realistic environment of the left and right side of the heart [30]. According to the researchers, the Cardiac Biosimulator is very useful to visualise the performance of a cardiovascular device in a pressurised heart with realistic hydrodynamics, heart wall movement and heart valve opening and closing. Furthermore, it allows to assess the functionality, implantability, and operability of a device. It would be great if experiments of this study could be performed on this Cardiac Biosimulator to assess above-mentioned performances.

Another option for estimating the effect of SMA-wires in a dynamic situation, will possibly be to create a mathematical model. However, it is questionable if all variables and data can be found in literature and the need of extra measurements in a physically dynamic model will be unnecessary.

Implementation of the device in the clinic will mainly depend on the proved safety and the ability to meet the required power supply. When further research can demonstrate that the required power can be delivered in such way that it is not too aggravate and it is safe for a patient, one can think about the optimal application for the device. It would for example be ideal if a device can be made based on a MRI-scan of the patient.

A cardiac MRI provides information of the left and right ventricle function, by measured values for end-diastolic volume (EDV), end-systolic volume (ESV), stroke volume (SV) and EF. Furthermore, segmental wall motion abnormalities can be determined with MRI. This information could show which segments of mostly the left ventricle, could benefit from additional support of SMAs. Another advantage of a MRI-scan is that it makes possible to

fabricate a 3D model of the heart, which can be a good tool to make a kind of exoskeleton for the SMAs to prevent dead spaces between the device and heart wall.

Measurements of absolute temperatures of SMA-wires would be more accurate when using a thermal camera with a higher resolution. Another option is probably to use scanning thermal microscopy.

Although an EF of 5% was not reached with the static heart model in this study, there is good hope that by improving the model (i.e. make it smaller in size and dynamically) and optimal use of created force by the SMAs a higher EF will be reached.

5 Conclusion

This study proved that it is possible to displace volume with SMA-wires in a static heart model. Furthermore, it gave insight in factors (like design, duty cycle, frequency, pulse intervals, diameter and insulation) which influences the effect of activation of SMAs. Despite the fact that an EF of 5% was not reached and this study has its limitations, recommendations were made to optimise experiments, resulting in a higher EF. Finding solutions for challenges such as optimal power supply, will determine if using SMAs in patients with heart failure will be preferable in the future, compared to already existing treatment methods.

Appendix A: Medical background

6

6.1 Anatomy of the heart

The main function of the heart is to pump blood to the tissues and organs of the human body. This section will further explain the anatomy of the heart and how it fulfils its main function, pumping blood through the human body.

6.1.1 Layers of the heart

The heart consist of three layers, from outside to inside the heart: the epicardium, myocardium and endocardium. The epicardium is also called the visceral pericardium and is the outer layer of the heart. The pericardium protects the heart against infections and keeps the heart in position. The myocardium, which is the middle layer of the heart, is the thickest layer of the heart in which cardiac muscle cells, cardiomyocytes, are located. The inner layer of the heart, the endocardium, mainly consist of endothelial cells and controls myocardial function.

6.1.2 Cardiac muscle cells

The structure of the cardiac muscle differs from skeletal muscle. The length of cardiac myocytes (about 100 μm) are for example smaller than skeletal muscle myocytes, which can be many centimeters long. Furthermore, cardiac myocytes are branched and connected to each other by intercalated disks, see Figure 19. In contrast to skeletal muscle myocytes, electrical conduction in cardiac muscle myocytes takes place from cell-to-cell. This electrically linkage between cardiac muscle myocytes is formed by gap junctions, which are located within the intercalated disks. As can be seen in Figure 19, individual cardiac myocytes

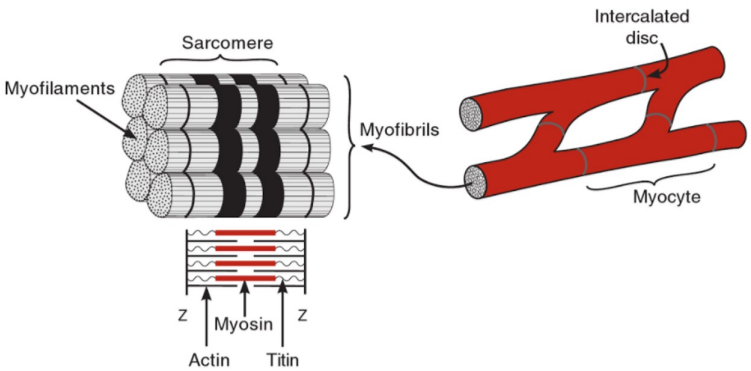

Fig. 19: Structure of cardiac myocytes. Cardiac myocyte consist of myofibrils, which contains myofilaments. The sarcomere lies between tow Z-lines. Adapted from: [31].

consists of myofilaments which are bundeled in so called myofibrils. These myofibrils are build up by the basic contractile unit, the sarcomere, which is bounded between two Z-disks. In normal conditions, each sarcomere ranges from 1.6 to 2.2 μm in length. Each sarcomere consists of thick and thin filaments, which are comprised of myosin and actin, respectively. As a result of interaction between actin and myosin, a sarcomere can shorten, and thereby shorten the distance between two Z-disks.

The length of the sarcomere is an important factor for the contraction force of a myocyte. This follows from the Frank-Starling Law, which states that "the energy of contraction is a function of the initial fibre length" [31, 32]. The Frank-Starling Law will be further explained in Subsection 6.3.3.

6.1.3 Chambers of the heart

Figure 20 shows the anatomy of the human heart. The heart contains of four compartments: the right atrium (RA), the right ventricle (RV), the left atrium (LA) and the left ventricle (LV). Atrioventricular valves are located between the atria and ventricles: the tricuspid valve between RA and RV, and the mitral valve between the LA and LV. The outlet valves of the right and left side are called the pulmonary valve and aortic valve, respectively. These heart valves makes sure that blood flows in the right direction. The RA receives venous blood from the superior vena cava (SVC) and the inferior vena cava (IVC). This blood is pumped from the RV to the lungs through the pulmonary artery. The blood becomes oxygenated in the lungs, after which it will flow into the LA by the pulmonary veins. Then, arterial blood will be pumped into the LV, which pumps it into the aorta for circulation to the rest of the body.

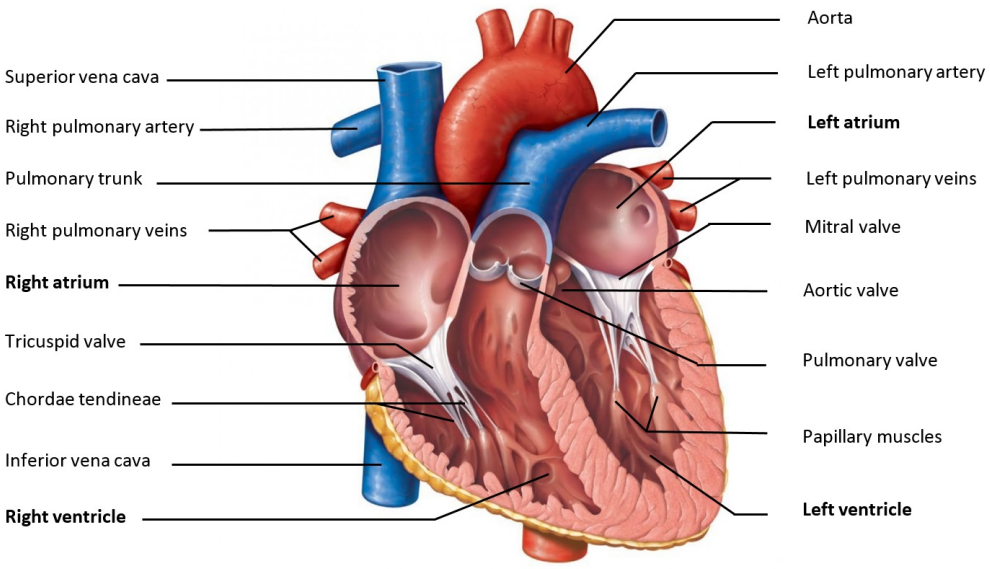

Fig. 20: Anatomy of the heart. Venous blood enters the RA via SVC and IVC and will be pumped to the RV. Blood becomes oxygenated in the lungs after is is pumped from the RV via the pulmonary artery. Arterial blood enters the LA via pumonary veins and will be pumped into the LV, from where it will be pumped into the aorta for circulation of the rest of the body. Adapted from: [33].

6.2 Physiology of the heart

6.2.1 Electrophysiology of cardiac cells

The group of cells in which the initial stimulus for activation of the heart takes place, is called the sinoatrial (SA) node, which is located in the RA. These cells can produce an electrical impulse spontaneously and are the heart's natural pacemaker-cells. The activation wave spreads from the SA node through the RA and LA to the atrioventricular (AV)-node. From this AV-node further conduction of the electrical impulses passes the His bundle, which has a left and a right bundle branch and causes the electrical activation of the ventricles.

6.2.2 Cardiac cycle

During every heartbeat, a sequence of mechanical and electrical events occur. This specific sequence is called "the cardiac cycle" and can be divided into four phases: inflow phase, isovolumetric contraction, outflow phase and isovolumetric relaxation, as can be seen in Figure 21 [32, 34]. Furthermore, this figure illustrates the left ventricular volume and pressures during these four phases. The isovolumetric contraction and outflow phase together constitute the ventricular systole in which blood moves from the LV to the aorta. Ventricular systole starts when ventricular pressure exceeds the atrial pressure of the LV and the mitral valve closes. Because mitral and aortic valves are both closed, pressure in the LV rises rapidly during the isovolumetric contraction phase. Finally, the ventricular pressure will exceed the aortic pressure, which results in opening of the aortic valve and start of the outflow phase. During the first part of this outflow phase, the rise of ventricular pressure continues and the volume of the LV reduces, because blood flows into the aorta. When ventricular volume decreases less rapidly, aortic and ventricular pressure also decreases.

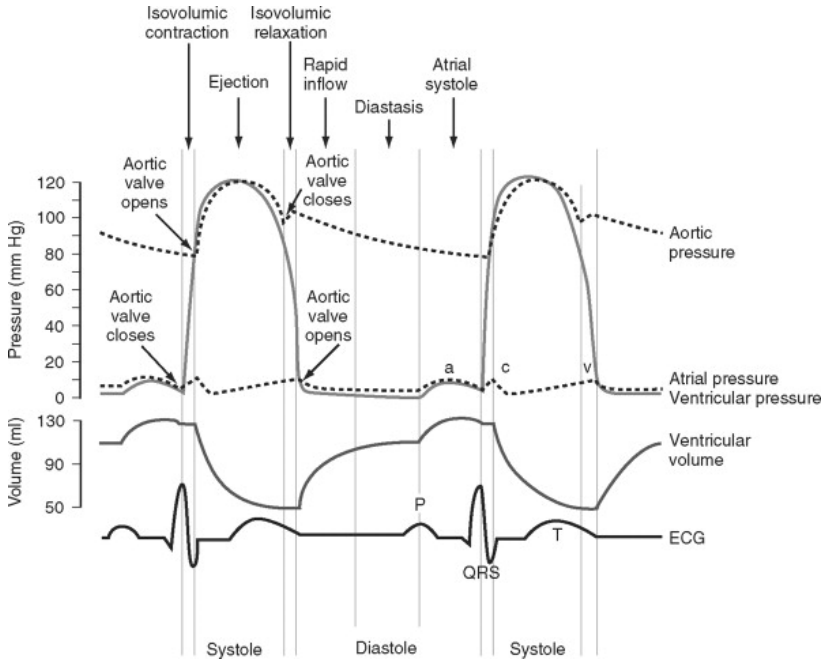

Fig. 21: Pressures and ventricular volume of the left side of the heart during cardiac cycle. Adapted from: [34].

When the aortic valve closes, the outflow phase is followed by the isovolumetric relaxation phase, which together with the inflow phase constitute to ventricular diastole. During the first part of the ventricular diastole, the mitral and aortic valves are closed and isovolumetric relaxation takes place, in which the ventricular pressure decreases rapidly. When the mitral valve opens, which happens when LV pressure becomes lower than left atrial pressure, the inflow phase starts and volume of the LV increases rapidly. The end of the inflow phase completes the cardiac cycle and the same sequence of mechanical and electrical events will occur during the following heartbeats.

6.2.3 Pressure-volume loop

Figure 21 shows the LV volume and pressure against time. Combining these two graphs, results in a so called pressure-volume loop, see Figure 22 [35]. The different phases of the cardiac cycles are also present in this loop. For example, the ventricular filling phase starts at point A (ESV) and ends at point C (EDV), isovolumetric contraction takes place between point C and D, the ventricular ejection phase between point D and F and the isovolumetric relaxation takes place between point F and A, which completes the cardiac cycle. Furthermore, the loop is bordered by the end-diastolic pressure-volume relation (EDPVR) and the end-systolic pressure-volume relation (ESPVR).

Multiple parameters can be determined from this pressure-volume curve. Stroke volume can for example be determined by measuring the distance between point A (ESV) en C (EDV). The slope of the ESPVR line is called E_{max} and is an indication of the contractility of the LV. Contractility indicates the intrinsic strength of the ventricle which is independent of external circumstances imposed by preload (i.e. EDV) or afterload (the force against which the ventricle must eject blood).

The EDPVR line presents the passive filling of the ventricle and the reciprocal of the slope of this curve is an indication of the ventricular compliance. Compliance describes how easily a

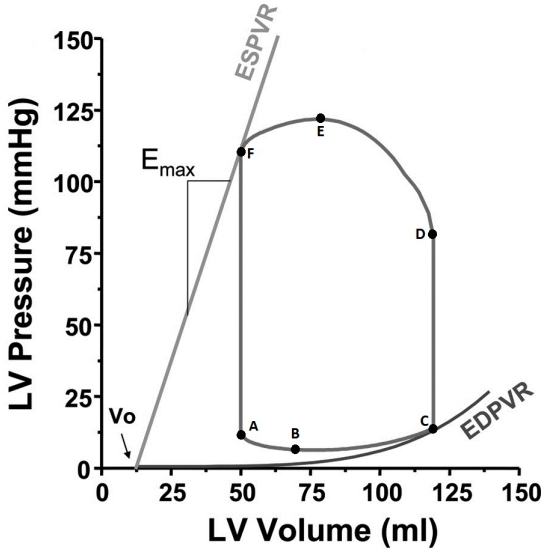

Fig. 22: Pressure-volume loop of the left ventricle. Point A represents ESV and point C EDV. Phases between the other points are mentioned in text. Adapted from: [35].

ventricle expands during volume filling. An increase in ventricular compliance will cause an increase in ventricular volume for a given filling pressure. This in turn will result in a higher EDV.

$$\text{Ejection fraction} = \frac{EDV - ESV}{EDV} \cdot 100\% \tag{6.1}$$

The relation between EDV and ESV is given by the SV, namely $SV = EDV - ESV$. From these components, the EF can be calculated (see Equation 6.1). Furthermore, SV and the heart rate (HR) determine the cardiac output (CO), which represents the amount of blood pumped by the heart per minute ($CO = SV \cdot HR$). The earlier mentioned Frank-Starling law states that when EDV increases, the CO of the heart increases as well. This Frank-Starling mechanism can be presented with a curve, which is shown in Figure 23 with a blue line for the normal situation. Changes in ventricular contractility and afterload can influence this Frank-Starling curve. A shift up can for example be caused by an increase in ventricular contractility or a decrease in afterload, see green line in Figure 23. Conversely, a decrease in contractility or an increase in afterload will shift the curve downwards, represented with the red line of the figure.

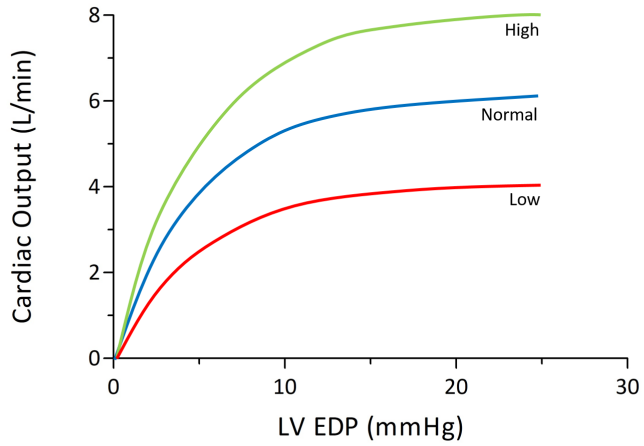

Fig. 23: Frank-Starling curve. A shift upwards (green line) from the normal situation (blue line) can be caused by an increase in contractility or decrease in afterload. A shift downwards (red line) can be caused by a decreased contractility or increased afterload.

6.2.4 Normal left ventricular motion

For developing a device which should support a failing heart, it is essential to know how the shape of a normal heart (and specifically the LV) changes during systole and diastole and how this is changed in case of a dilated LV.

The normal shape of the LV has been described as a prolate ellipsoid [36]. Specific contraction of muscle layers of the heart makes it possible that the LV can deform and achieve twisting and squeezing motions. Multiple studies describe the arrangement of the heart fibres as a right-handed helix and circumferential arrangement in the subendocardial area and as

a left-handed helix in the subepicardial area [37–40]. Holdrege et al. made a schematic representation of the heart fibres in the LV, see Figure 24 [41].

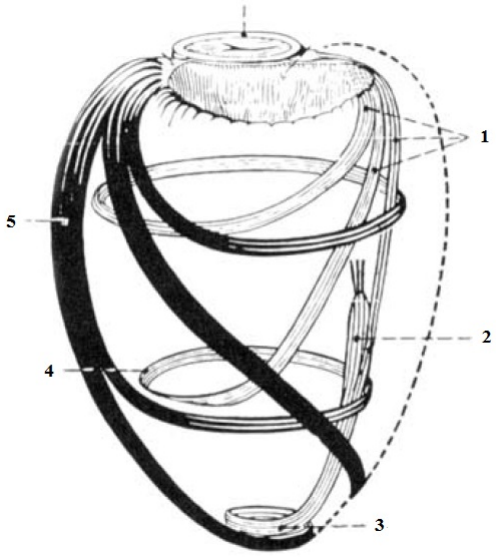

Fig. 24: Fibre orientation of the left ventricle (adapted from: [41]). 1= subendocardial fibres, 2= papillary muscle, 3= vortex cordis, 4= circumferential fibres, 5= subepicardial fibres.

Sengupta et al. presented a clear overview of the sequence of twist mechanics of the LV, which is shown in Figure 25 [18]. During isovolumic contraction, a clockwise rotation of the apex and counterclockwise rotation of the ventricular base will be produced by shortening of the subendocardial myofibres and stretching of the subepicardial myofibres (see Figure 25A).

During the ejection phase, the subendocardial and subepicardial myofibres shorten simultaneously, which causes a counterclockwise rotation of the apex and a clockwise rotation of

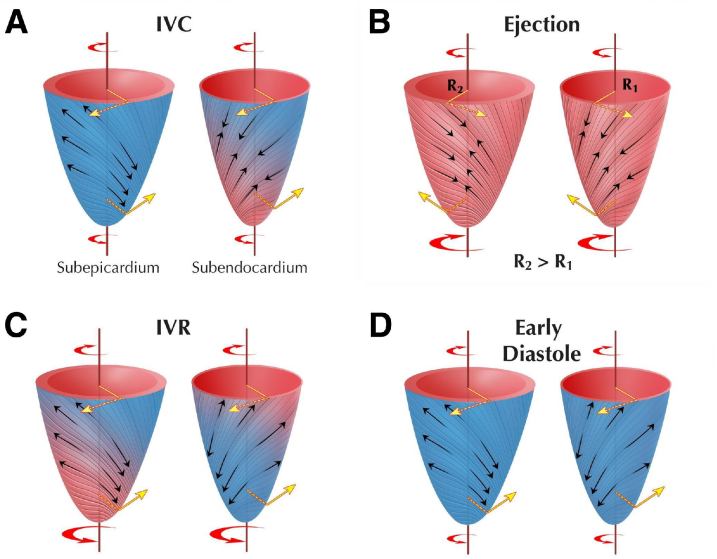

Fig. 25: Twist mechanics of LV. During isovolumic contraction (A), ejection phase (B), isovolumic relaxation (C) and early period of diastole (D). Adapted from: [18].

the ventricular base (see Figure 25B). The situation during isovolumic relaxation is shown in Figure 25C. During this phase, the subendocardial myofibres lengthens from apex toward the base, while supepicardial myofibres lengthens from base to apex. Relaxation of both myocardial layers occurs during the early period of diastole (see Figure 25D).

6.3 Heart failure

As mentioned in Section 1.2, there are multiple types of HF. This section will give a more detailed insight in heart failure with reduced ejection fraction (HFrEF) and dilated cardiomyopathy (DCM), which is a common condition within this HFrEF group.

6.3.1 Incidence and prevalence

In West-European countries, HF is increasingly prevalent, affecting 1% - 2% of the total population and an incidence of approximately 5-10 per 1000 people per year [6] . In the Netherlands, 1% (± 130.000) of the adult population suffers from HF, which will increase to 195.000 in 2025.

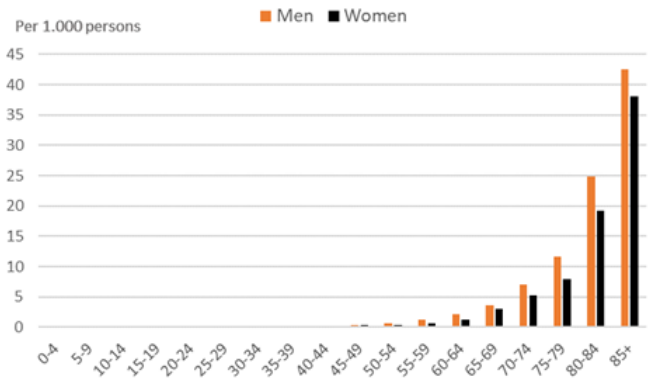

Fig. 26: Incidence of Heart Failure in Dutch general practice for several age groups. Data adapted from: [42].

The Dutch government institute for public health and environment, the RIVM, did some research to the incidence of HF in Dutch general practice [42]. In 2015, approximately 40.000 new patients were diagnosed with HF. For the different age groups, incidence rates turned out to be higher for men than for women, as can be seen in Figure 26.

6.3.2 Causes

HF is a complex clinical syndrome, which can be caused by many conditions. The various causes of HF can be classified in five categories:

1. Primary myocardial disorders
2. Increased volume load of the heart
3. Increased pressure load of the heart

4. Inflow obstruction of the heart
5. Arrhythmias

Table 3: Causes for development of heart failure [43].

Main cause	Examples
Myocardial	- Coronary artery disease - Cardiomyopathy - Myocarditis
Volume load	- Overload - Valve insufficiency - Aneursm of the left ventricle - Ventricular septal defect - Atrial septal defect
Pressure load	- Systemic or pulmonary arterial hypertension - Aorta valve stenosis - Hypertrophic cardiomopathy - Pulmonary valve stenosis
Inflow obstruction of ventricles	- Pericarditis with pericardial fluid and tamponade - Constrictive pericarditis - Mitral or tricuspid valve stenosis - Restrictive cardiomyopathy - Hypertrophy (at hypertension)
Arrhythmias	- Tachycardia or extreme bradycardia - Atrial fibrillation

The most common causes of these five categories are summarised in Table 3.

Primary myocardial disorders

One of the causes of HF can be caused by function loss of individual muscle fibres of the heart. This is for example the case when cardiac muscle fibres are replaced by connective tissue due to an infarct. Overload of the remaining cardiac tissue to compensate for loss of cardiac tissue will have negative influence on the cardiac pump function. Another cause of a primary disorders is inflammation of the heart muscle, for example due to a virus or bacteria, also called myocarditis. A primary cause which is caused by the myocard itself and can be genetically determined, is called cardiomyopathy. The defect can be located in the contractile element, but also in connective tissue elements which surrounds individual cardiomyocytes.

Increased volume load of the heart

An increased volume load of the heart is mainly caused by heart valve disorders, such as mitral insufficiency and aortic insufficiency. In case of mitral insufficiency, the LV will have an increased volume, because a part of the ejected stroke volume will flow back to the LA during systole, which will then flow back to the LV during diastole. In case of aortic insufficiency, blood will flow back from the aorta to the LV during diastole. Less common causes of an increased volume load of the heart are ventricular septal defect or atrial septal defect.

Increased pressure load of the heart

An increased pressure load of the heart can be caused by heart valve diseases, such as aorta valve stenosis and pulmonary valve stenosis. These heart valve diseases causes an obstruction of the outflow and the heart will be hypertrophic to compensate for the increased pressures and secure that enough blood will be pumped through the body. After a while, ventricles can not further compensate for this load and will decompensate, which will mostly result in dilatation of the ventricle(s). A long lasting hypertension will also lead to hypertrophy (mostly of the LV), which can also lead to HF.

Inflow obstruction of ventricles

Just like outflow obstruction, inflow obstruction of the heart can also lead to symptoms of HF. For example, due to heart valve diseases such as mitral or tricuspid valve stenosis. In case of mitral valve stenosis, obstruction of blood flow from LA to LV (during diastole), will finally lead to an increase in pressure of the LA and secondary to increased pressures in pulmonary vasculature and RV. Because of the reduced inflow to the LV, SV will also decrease. In case of tricuspid valve stenosis, the inflow of blood is obstructed from the RA to the RV. Other less frequently seen causes of inflow obstruction of ventricles are pericarditis or a tumor.

Arrhytmias

Another important cause of HF are arrhythmias. Increased heart rate (tachycardia) which exist for a large part of the day, can for example cause exhaustion of myocardial cells which can lead to increased energy and oxygen requirements, which can lead to a reduced myocardial function. Also decreased heart rates (bradycardia) can lead to HF, for example in case of a atrioventricular block. In some cases this can be treated with CRT, which will be explained in Subsection 6.3.5.

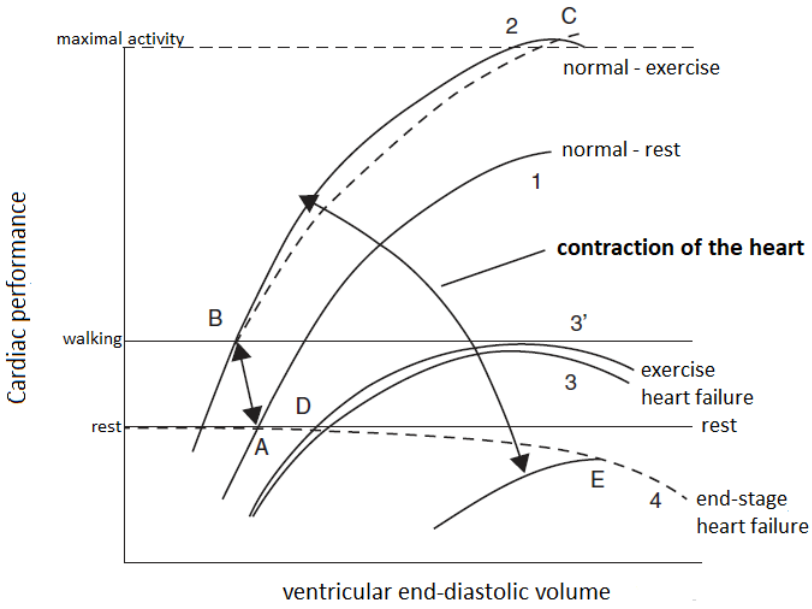

Fig. 27: Frank-Starling curve for normal and failing hearts. Adapted from: [44].

6.3.3 Pathophysiology

When cardiac tissue is damaged and suddenly no longer meets the tissue requirement for blood (and nutrients), a number of compensation mechanisms can start to maintain cardiac output and peripheral perfusion [45]. However, these mechanisms become pathophysiological as HF progresses. CO (SV x HR) can be maintained by an increase in HR or SV.

Frank-Starling mechanism

Increase of SV can be accomplished by the Frank-Starling mechanism, in which an increased end-diastolic volume leads to an increased heart contractility. However, at a certain moment the ventricle is not capable to resolve the increased volume. Increased EDV will then lead to left or right decompensatio cordis. The Frank-Starling curve for normal and failing hearts, is shown in Figure 27. In the normal situation, an increased contractility (for example due to exercise) will lead to an increased CO without extreme rise in elongation of muscle fibres, see point 1 to point 2 in Figure 27. In case of HF, contractility can only increase with increased EDV and filling pressures as a consequence (point 3 and 3'). In severe HF only a small increase in contraction occurs, which cost a strong increase in LV fillings pressure and induces the risk of pulmonary edema.

Shape and movement of left ventricle in case of dilated cardiomyopathy

Figure 25 shows the motion of the LV under normal circumstances. Motion of the LV changes in case of a heart disease. Sengupta et al. assessed rotation of the apex and base of the left ventricular, as well as the net LV twist angle, with speckle-tracking echocardiography [18]. Figure 28 shows the different rotations for a normal subject (Figure 28A) and for a patient with dilated cardiomyopathy with systolic heart failure (Figure 28B).

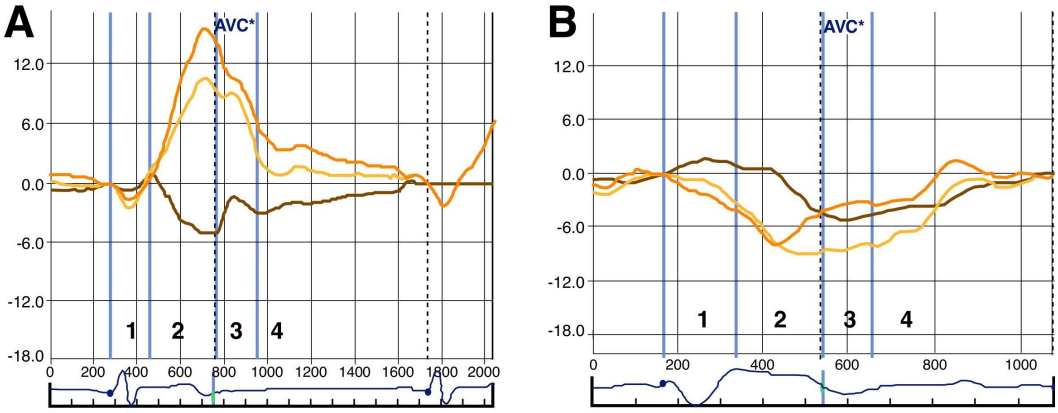

Fig. 28: Twist of the apex, base of the left ventricle and the net twist angle (shown in yellow, brown and orange, respectively) during isovolumic contraction (phase 1), ejection (phase 2), isovolumic relaxation (phase 3) and early diastolic filling (phase 4). A) A normal subject. B) A patient with dilated cardiomyopathy with systolic heart failure. AVC = aortic valve closure. Adapted from: [18].

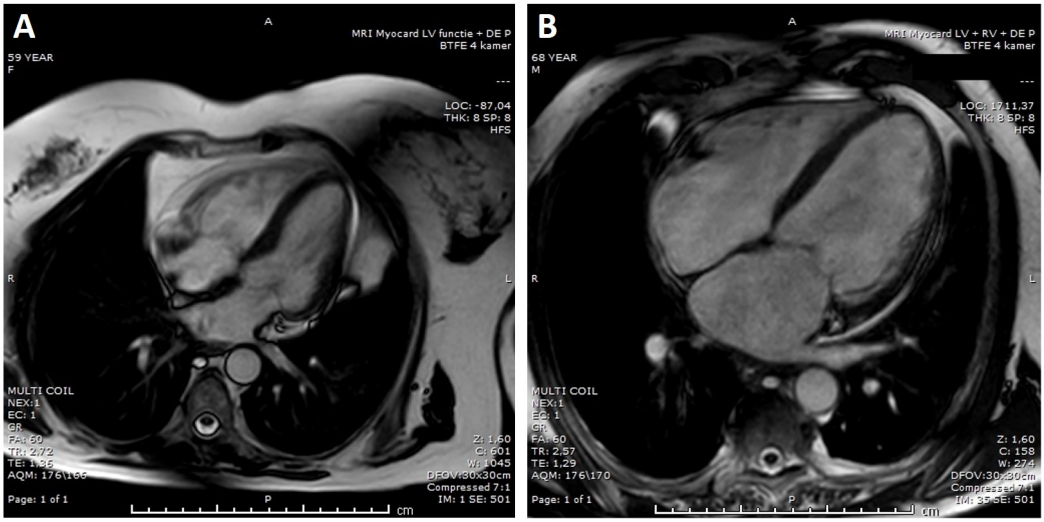

Fig. 29: Cardiac MRI-scans. A) Normal heart with good left ventricle function (EDV: 75 mL, ESV: 18 mL, SV: 56 mL, EF: 75%). B) Dilated left ventricle with dysfunction (EDV: 310 mL, ESV: 271 mL, SV: 40 mL, EF: 13%).

6.3.4 Diagnosis

As mentioned before, one speaks of HFrEF when clinical symptoms of heart failure are present and a LVEF <40% is measured. Furthermore, biomarkers are also widely used for the diagnosis. A well-known biomarker for heart failure is B-type natriuretic peptide (BNP). BNP is secreted by ventricular myocytes when the ventricular filling pressure is elevated [46]. Another biomarker which is frequently measured is NT-pro B-type natriuretic peptide (NT-proBNP). NT-proBNP is a biologically inactive fragment, which is released in the circulation when BNP is cleaved from the pro-hormone proBNP [47]. These biomarkers indicates heart failure, when the concentration of BNP and NT-proBNP are elevated. The normal upper limit value for BNP is 35 pg/mL and 125 pg/mL for NT-proBNP [5].

Subsequently, echocardiography is widely used to establish the diagnosis, because it can provide information about wall thickness, volume of the atria and ventricles, the function of the heart valves and the ventricular function during systolic and diastolic phase. Another form of cardiac imaging is MRI, which is useful to assess the severity of ventricular dilatation, dysfunction, and contraction abnormalities, for example in patients with DCM [48]. Figure 29 shows a MRI-scan of a patient with a normal heart (29A) and a MRI-scan of a patient with DCM (29B).

6.3.5 Treatment

The aims of treatment of patients with HF are to improve their clinical condition and quality of life, to prevent admission to the hospital and reduce mortality [3]. In patients with HFrEF, clinicians can use the advised treatment strategy, as described in the ESC guidelines, [5]. This treatment strategy, which is shown in Figure 30, gives a recommendation for the right moment for treatment with specific medication and devices. The different kinds of medication and devices are briefly described below.

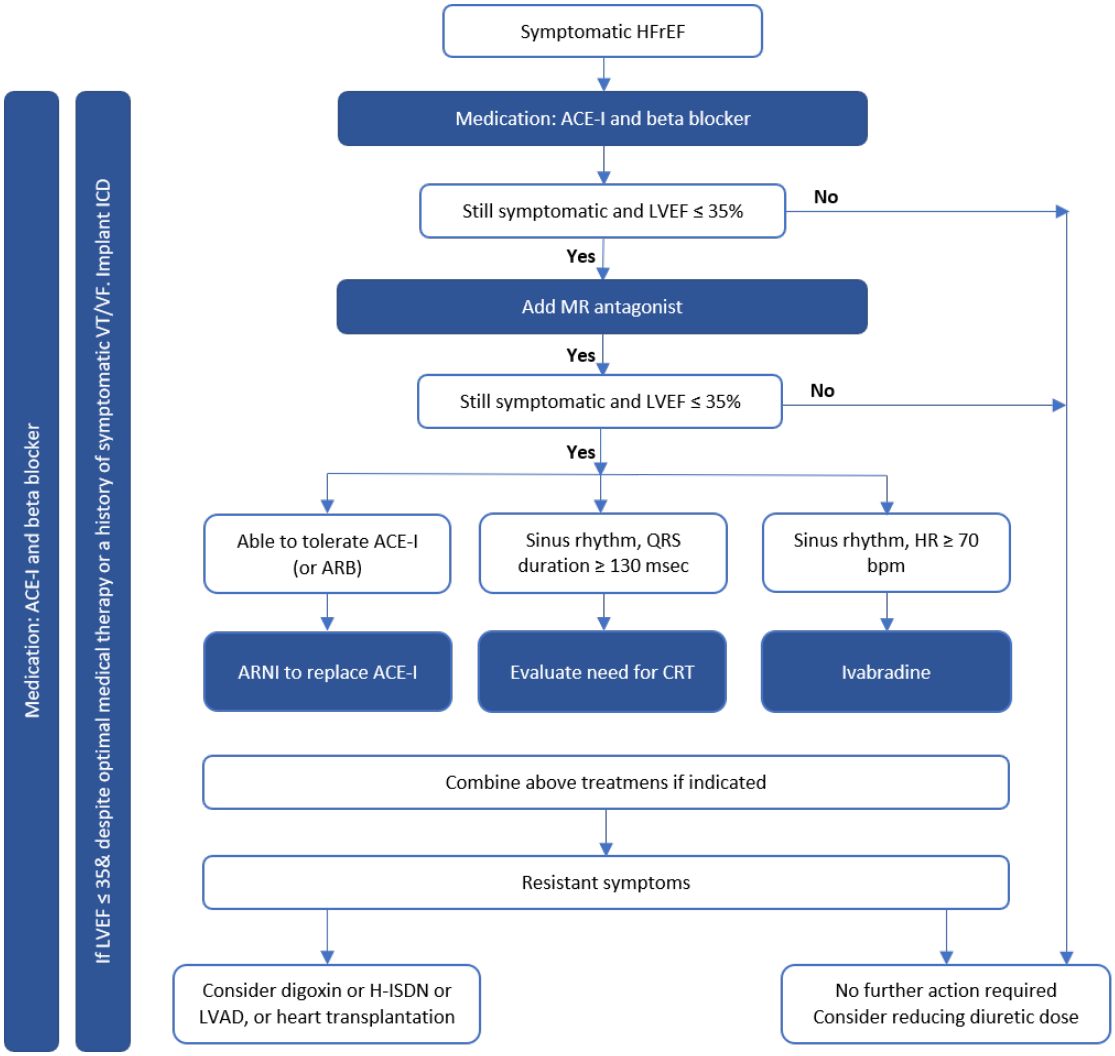

Fig. 30: Algorithm for treatment of HFrEF patients. Redrawn from: [3].

Medication

As can be seen in the treatment algorithm in Figure 30, treatment of HF starts with medication. Except for contraindication, angiotensin-converting-enzyme inhibitors (ACEIs) are recommended in every HFrEF patient. ACEIs reduces vasoconstriction and therefore lowers blood pressure and thus improves heart function. Beta-blockers lowers heart rate and are as well recommended in every HFrEF patient. Besides ACEIs and beta blockers, diuretics are recommended to improve symptoms such as dyspnea and edema.

If symptoms are still present with diuretics, ACEIs and beta-blockers, it is recommended to prescribe mineralcorticoid receptor antagonists (MRAs), which lowers high blood pressures and should reduce chance of hospitalisation and death.

A drug which should be considered in symptomatic patients with a heart rate $\geq$ 70 bpm in rest and a LVEF $\leq$ 35% in spite of treatment with beta-blocker, ACE-I and MRA is Ivabradine. Ivabradine inhibits the I_f channel in the sinus node and therefore slows the heart rate.

Implantable cardioverter-defibrillator

Most patients can be treated effectively with optimal medical treatment. However, the incidence of sudden death, mostly caused by ventricle fibrillation or ventricle tachycardia, in patient with HF is high. An implantable cardioverter-defibrillator (ICD) reduces the risk of sudden death, and is recommended in patients in which optimal medical therapy has failed to increase LVEF to $> 35\%$ within three months [5].

Cardiac resynchronisation therapy

When contraction of the LV and RV are out of phase due to a delayed conduction (i.e. with left bundle branch block), the pump function of the heart becomes less effective. A therapy in which an atrial, right and left ventricle pacing electrode is placed to improve filling and contraction pattern, is called CRT. Patients are eligible for CRT, if the following criteria are met [5]:

1. A reduced pump function of the heart (LVEF $\leq 35\%$);
2. A broadened QRS-complex due to conduction delay (≥ 130 ms);
3. Symptomatic heart failure (NYHA-class $\geq$ II).

CRT is able to extend or shorten the stimulation time between RV and LV, which makes it for example possible to abrogate the dissynchrony of a left bundle branch block [50]. There are two types of CRT-devices: a CRT-P (pacemaker) and a CRT-D (defibrillator). A CRT-D is a biventricular pacemaker which has an additional ICD function, which can be applied by a RV shocking electrode.

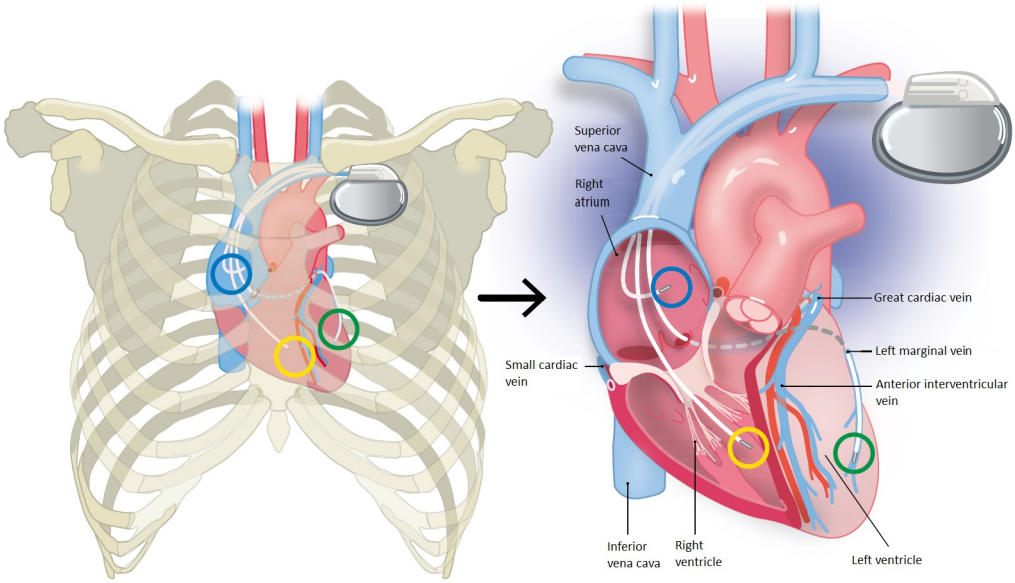

Fig. 31: Location of pacing electrodes for cardiac resynchronisation therapy (CRT), adapted from: [49]. Right atrial, right ventricle and left ventricle electrode are indicated with a blue, yellow and green circle, respectively.

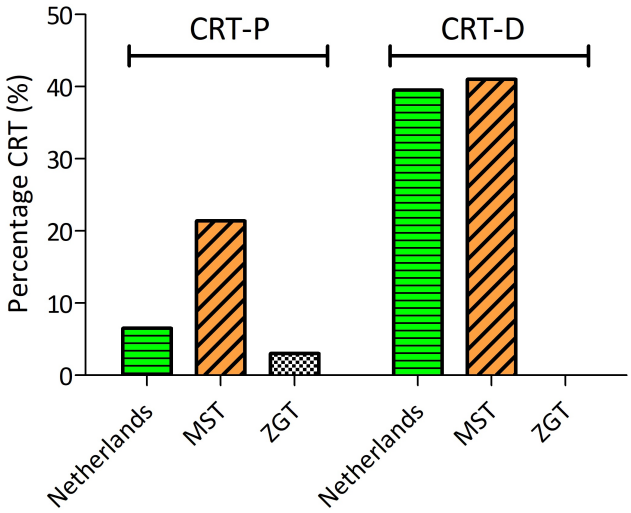

Fig. 32: CRT implantations in proportion to regular pacemaker and ICD implantation in 2015. Proportion of implantations for Dutch hospitals in general and Medisch Spectrum Twente (MST, Enschede) and Ziekenhuis Groep Twente (ZGT, Almelo/Hengelo) Source: [51] .

Implantation of a CRT-device takes place under local anesthetics and lasts for about two hours. The pacing electrodes are introduced via the cephalic vein or subclavian vein, whereafter the device is placed under the clavicle, see Figure 31 [49]. The figure shows also the location of the atrial, right and left ventricle pacing electrode, indicated with a blue, yellow and green circle, respectively. The LV electrode is positioned through the coronary sinus in a venous side branch at the height of the posterolateral wall of the LV. In case of a failed positioning, the pacing electrode can be positioned epicardial on the heart as well.

The fraction of CRT and ICD implantation relative to implantation of regular pacemaker or ICD for Dutch hospitals in 2015, is shown in Figure 32. It shows that in Dutch hospitals proportionately more regular pacemakers and ICDs were implanted and that for Medisch Spectrum Twente (MST) hospital the proportion of CRT-D to regular ICD was twice as large as the proportion of CRT-P to regular pacemakers [51].

Surgical treatment

For a long time, heart transplantation was the only surgical treatment for a small percentage of patients with severe congestive HF. The small number of available donor hearts, side effects due to immunosuppression and a high hospital mortality and morbidity where reasons to develop new alternative treatments. This subsection will give an overview of several surgical treatment options for patients with HF.

Cardiomyoplasty

Cardiomyoplasty is a surgical procedure in which the failing heart is wrapped to provide support. Both dynamic and passive cardiomyoplasty are reported in literature. In 1985 Carpentier et al. introduced dynamic cardiomyoplasty, in which they wrapped the latissimus dorsi muscle around the heart and stimulated this muscle for support of the heart contraction [52]. However, in a clinical study which investigated the efficacy of dynamic cardiomyoplasty

it was suggested that improvement in ventricular contraction was not derived primarily from active stimulation of the latissimus dorsi muscle, but from the passive girdling of the heart which limits the progression of ventricular dilatation [53]. This procedure is barely performed now.

Besides the dynamic cardiomyoplasty, some researches investigated passive cardiomyoplasty as a method to reduce ventricular dilatation. A product that has been studied extensively, is the CorCap cardiac support device (Acorn Cardiovascular, Inc.). The CorCap device is a mesh of polyester, which is placed from the apex to the atrioventricular groove of the heart (see Figure 33). The CorCap is circumferentially placed around both ventricles and prevents progression of LV dilatation and thereby reduces LV wall stress [54]. Implantation of the CorCap device is performed in only a few heart surgery centers in the world.

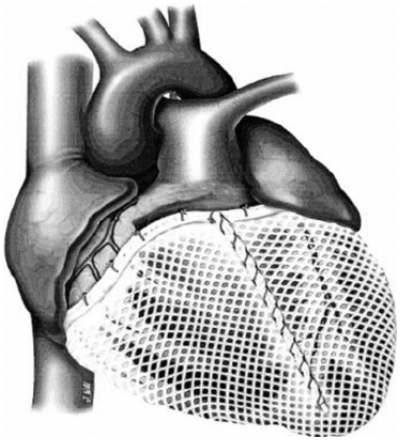

Fig. 33: CorCap Cardiac support Device (Acorn Cardiovascular, Inc.).

Left ventricular reduction

A well known surgeon who pioneered a new surgical treatment for patients with end-stage congestive HF is Dr. Randas Batista. He supposed that surgical reduction of the LV might recover the mechanical function of the heart.

During the Batista procedure, an incision is made from the apex toward the base of the LV [55]. The distance between the two papillary muscles of the LV should be determined, whereafter a flap of the myocardium can be removed, leaving the papillary muscles intact. The incision is closed with a single layer suture, followed by a second hemostatic suture and removing air from the LV.

The Batista procedure, also called partial left ventriculectomy (PLV) or ventricular remodeling, reduces the LV volume and is based on Laplace's law. Laplace's law states that $T = P \cdot R$, where T is the wall tension, P is the cavitary pressure, and R is the radius of the chamber. In case of dilated cardiomyopathy, the radius of the LV is increased and thus leads to an increased wall tension. Conversely, a reduction of the radius of the ventricle will decrease the wall tension, according to Laplace's law.

A treatment device which is probably based on Batista's procedure, is the Myosplint (Myocor Inc.). The Myosplint consist of multiple buttons which are placed transversely through the LV, perpendicular to its long axis, see Figure 34. Tightening of the buttons of the device

causes a reduction of the radius of the ventricle. According to the earlier mentioned Laplace's law, the Myosplint reduces wall stress and thereby improves ventricular function [56].

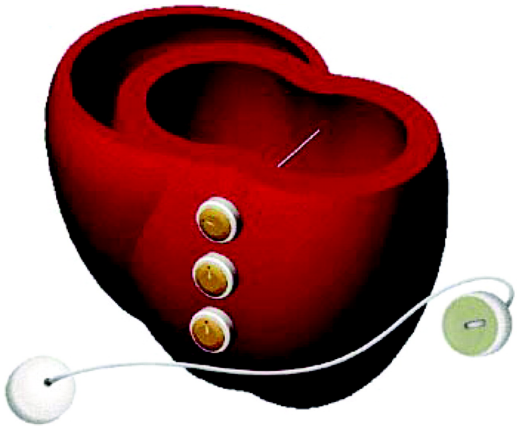

Fig. 34: Myosplint (Myocor, Inc.). Tightening of the three buttons of the device causes a reduction in radius of the ventricle.

Mechanical devices to assist the heart

Another option for patients with end-stage HF, is a LVAD. A LVAD assist the LV by removing blood from the ventricle to deliver this blood to the aorta, through a pump. The LVAD is developed and approved as a bridge to heart transplantation, however nowadays there is a trend towards using LVADs as a destination therapy [57].

Over the years, three generations of LVADs are developed. The first generation LVADs were based on pulsatile pump systems and the use of valves for outflow and inflow. These pumps are driven by a pneumatic drive system and implanted under the diaphragm in a intra-abdominal or a preperitoneal pocket below the rectus abdominis. The LVADs of these generation has a big volume, which increases the risk of infections.

Fig. 35: Heartmate II (Thoratec Inc, Pleasanton, CA). A second generation LVAD, which consists of an axial flow pump.

The second generation of LVADs includes pumps which deliver a continuous flow, that offer multiple advantages over pulsatile flow pumps of the first generation. The pumps are for example smaller in size, which reduces the risk of infections and makes it easier to implant the device. Furthermore, the pump has fewer moving parts (valves are for example

not needed for continuous flow) and a reduced energy consumption, which improves the durability of these devices. The mostly used LVAD of this generation is the Heartmate II (Thoratec Inc, Pleasanton, CA), which is shown in Figure 35. The Heartmate II is an axial flow pump, which drains blood from the LV with an inflow cannula and has an outflow cannula to return blood to the aorta [58].

The third generation of LVADs are implantable devices with a centrifugal continuous flow pump. A well known LVAD of this generation is the HeartWare HVAD (HeartWare Inc, Miramar, FL), which is shown in Figure 36. The HeartWare is directly placed at the apex of the heart and the "outflow graft" is connected to the ascending aorta. Furthermore, the HeartWare is smaller than the other generations of LVADs and can be implanted in the pericardial cavity.

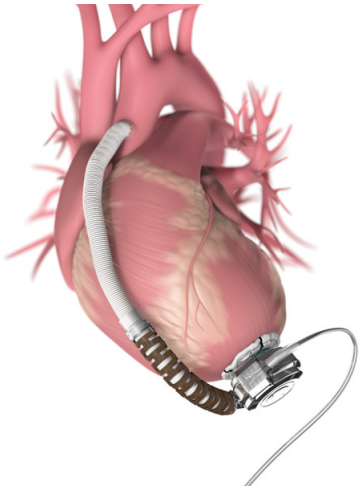

Fig. 36: The HeartWare HVAD (HeartWare Inc, Miramar, FL). A third generation LVAD, which consists of a centrifugal continuous flow pump.

7 Appendix B: Technical background

7.1 Smart materials

Smart materials are materials which have one or more properties that can be changed by external stimuli, such as stress, temperature, pH, light or electricity. There are multiple types of smart materials. Examples are shape memory alloys (SMAs) and shape memory polymers (SMPs), which are materials in which large deformation can be induced and recovered through temperature changes.

7.1.1 Shape memory alloys

SMAs are metallic alloys with two, three or four components, with special compositions. There are two main families of SMAs: the copper-based and NiTi-based SMAs. Although copper-based SMAs are less expensive than nickel-titanium-based SMAs, NiTi alloys have better thermo-mechanic performance and are therefore preferable for most applications [59].

Properties

Thermally responsive SMAs have two interesting properties: shape memory effect (SME) and superelasticity (SE) [60]. SME refers to the ability to return back to their predetermined shape upon heating. SE refers to the ability of SMAs to recover their shape after unloading of a large amount of inelastic deformations. Reversible phase transformations of SMAs are responsible for these two properties.

SMAs display two distinct crystal phases: the austenite phase at high temperature and the martensite phase at low temperature. Figure 37 shows the SME. When the alloy is cooled and completely composed of martensite, the SMA can be easily deformed. This phase is called the twinned martensitic phase (at point 1). After deforming the SMA by applying load, the crystal configuration changes from twinned to detwinned martensite (at point 2). This deformation remains, even after removing the load (from point 2 to 3). The martensite-start-temperature (M_s) is the temperature at which the transformation to the martensite starts and the temperature at which the transformation is complete, is called the martensite-finisch-temperature (M_f) [61]. The SMA changes into the austenitic phase (at point 4), when increasing the temperature. The temperature at which this transformation starts, is called the austenite-start-temperature (A_s) and the temperature at which the transformation is complete, is called the austenite-finish-temperature (A_f). The alloy recovers then to its original shape, which is maintained when the alloy cools down

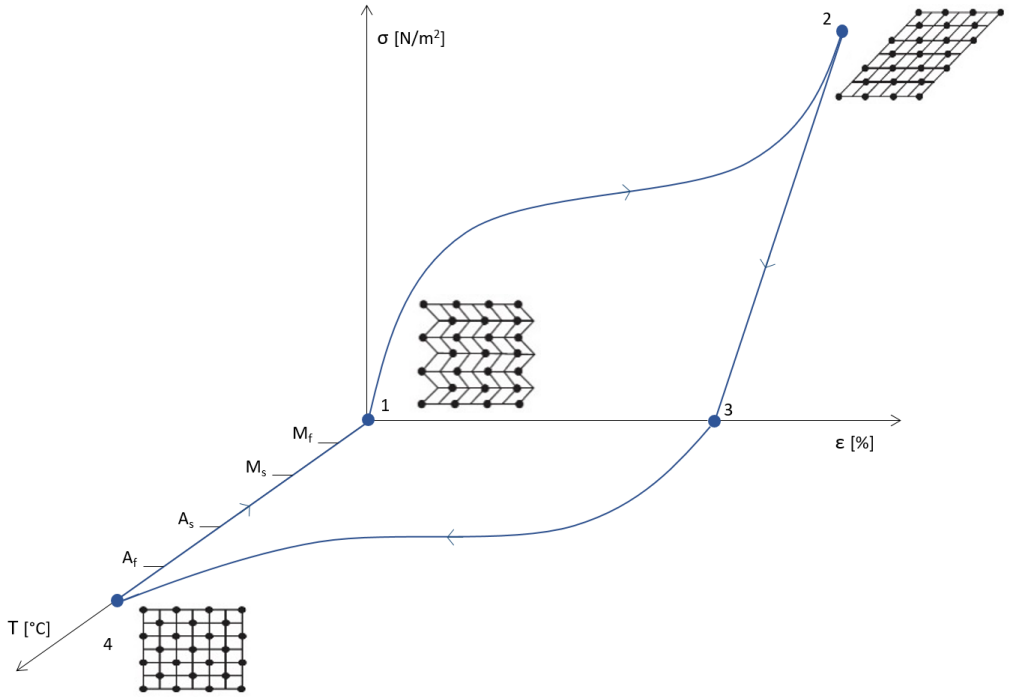

Fig. 37: Shape memory effect. A_s = austenite-start-temperature, A_f = austenite-finish-temperature, M_s = martensite-start-temperature and M_f = martensite-finisch-temperature. Redrawn from: [62].

(from point 4 to 1). The martensite phase is weak and can be easily deformed because of its parallelogram structure. By contrast, the austenite phase is relatively strong, because it has only one possible orientation. The ratio between the different particles of a NiTi based SMA determines the start and finish temperature of the martensite and austenitic phase. Start and finish temperatures of martensite and austenitic phase of different ratios of the particles in NiTi and NiTiCu alloys are listed in Table 4.

Bio-compatibility is extremely important for biomedical applications of SMAs. Leaching out of chemical elements, which is called toxicity, can for example cause several reactions in the human body such as: local tissue reaction, systematic toxic reaction, allergic reaction, and

Table 4: Several NiTi based SMAs with corresponding phase temperatures [63].

Alloy	M_s (°C)	M_f (°C)	A_s (°C)	A_f (°C)
$Ni_{49.99}Ti_{50.01}$	65.7	38.7	79.1	107.2
$Ni_{43.5}Ti_{51.5}Cu_{5.0}$	60.4	40.6	69.4	85.8
$Ni_{44.0}Ti_{51.0}Cu_{5.0}$	60.0	38.3	68.1	87.4
$Ni_{44.6}Ti_{50.4}Cu_{5.0}$	65.4	43.3	68.1	87.7
$Ni_{44.75}Ti_{50.25}Cu_{5.0}$	68.8	51.3	73.2	89.9
$Ni_{45}Ti_{50.0}Cu_{5.0}$	71.7	43.7	66.6	94.7
$Ni_{42.5}Ti_{50.0}Cu_{7.5}$	64.0	46.7	69.7	83.9

teratogenic, mutagenic and carcinogenic response [64]. According to multiple studies, NiTi is biocompatible and can therefore be used in biomedical applications [12, 65].

Limitations

Despite the many benefits of using SMA-wires, there are also some limitations of using these materials. One limitation of SMAs is for example their relatively slow cooling rate, caused by limited heat conduction and convection [66]. Rate of heating and cooling depends on the size of the SMA. Due to their higher resistivity, SMAs with a smaller diameter heat faster and due to their higher surface-to-volume ratio cooling is also faster in SMAs with a smaller diameter [17, 67]. On the other hand, the smaller the diameter size, the smaller the pulling force the SMA can create during contraction. A compromise between a fast heating and cooling and the pulling force, for selecting the SMA diameter depends therefore on the desired application.

An et al. investigated the influence of diameter on some characteristics in activated NiTi SMAs by electrical current [67]. They used Equation 7.1 to estimate the maximum temperature in the SMA.

$$T_{\max} = \frac{2B(e^{\frac{mL}{2}} - e^{\frac{-mL}{2}})}{m^2(e^{mL} - e^{mL})} + T_0 - \frac{B}{m^2} \tag{7.1}$$

where

$$m = 2\sqrt{\frac{h}{kd}}$$

$$B = -\frac{4I^2R}{\pi^2 kd^2}$$

Here, L is the length of the SMA-wire, d the diameter, h the convection heat transfer coefficient, k the thermal conductivity, R the resistance of SMA and I the passing electrical current. This equation makes it possible to assess the effect of the SMA diameter and could maybe be used in finding the optimal compromise.

Another limitation of SMAs is the low energy efficiency. The Carnot efficiency, which describes efficiency of conversion from thermal energy to mechanical work, of SMAs is approximately 10% [68]. There are several configurations of SMA actuators. In SMA-springs, a relatively small microscopic strain can generate large macroscopic displacements, but a larger material volume is needed to generate the same force compared to SMA-wires. Because SMA-wires generates more work with a minimal SMA material, they are preferred above SMA-springs.

Application of SMAs

Due to their high corrosion resistance [69], bio-compatibility [70] and non-magnetic properties [71], SMAs are very useful in biomedical applications. In addition to the use of SMAs in orthopedic applications, like bone plates and compression staples, SMAs are also used in cardiovascular applications. One example of a cardiovascular application are the SMA stents.

A stent makes it possible to retain the diameter of an artery, after stenosis blocks the blood flow due to atherosclerosis [64]. A little bit more complicated application of SMAs, is the use of SMAs in an artificial myocardium. Only a few studies investigated the use of SMAs in an artificial myocardial assist device for support of a failing heart [21, 23, 72].

Flexinol® from Dynalloy

The essential function of Flexinol® is to shorten in length and create motion or force when it is heated. Flexinol® is an SMA-alloy which consist of approximately 50% Nickel and 50% Titanium (exact values are not given by the manufacturer of Flexinol®). The ratio of Nickel and Titanium has influence on the amount of transformation cycles. A study of Bertacchini et al. showed that the number of transformation cycles increases with higher concentration of nickel [73]. However, the number of transformation cycles decreases when transformation occurs under high stresses. The specific temperature vs. strain curve of Dynalloy's Flexinol® is shown in Figure 38. Furthermore, specifications of Flexinol® is listed in Table 5.

Cooling methods

The cooling time is equal to the relaxation time. The easiest way to increase the cooling time is to use an SMA-wire with a smaller diameter. Because a smaller wire has a bigger surface-to-mass ratio. Other improvements in cooling time can be made by increasing stress on the wire,using a higher temperature wire, using forced air or heat conductive grease [17].

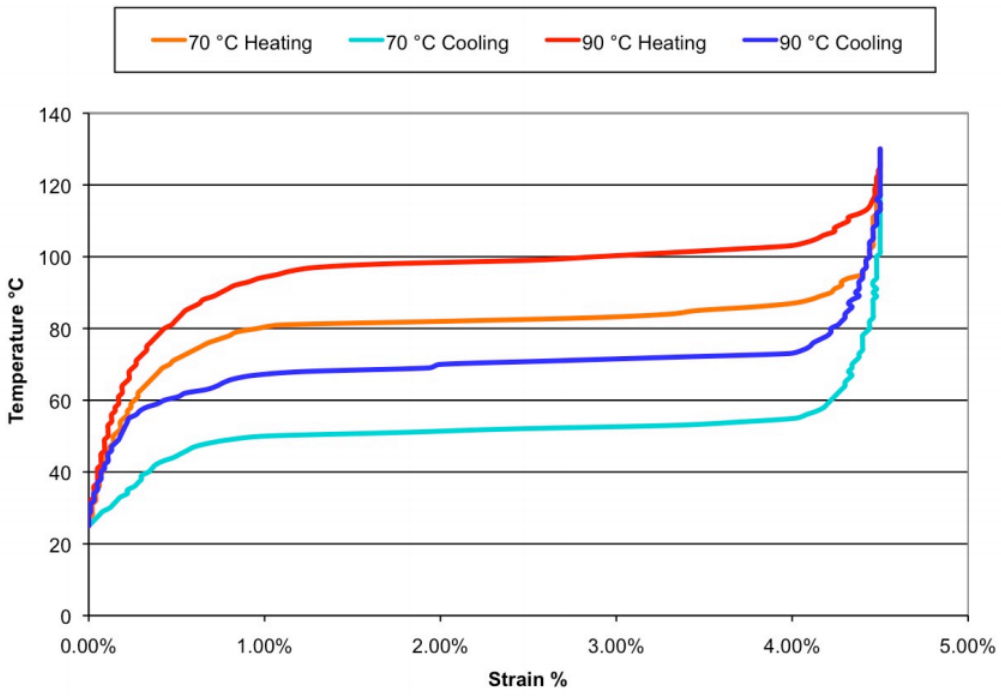

Fig. 38: Temperature-strain curve of Flexinol ®. Adapted from: [17].

Table 5: Specifications of Flexinol ® [17, 74].

Property	Value
Density	6.45 g/cm^3
Specific Heat	0.2 cal/g°C
Melting point	1300 °C
Heat of transformation	5.78 cal/g
Austenite start temperature (A_s)	67°C
Austenite finish temperature (A_f)	75°C
Martensite start temperature (M_s)	48°C
Martensite finish temperature (M_f)	38°C
Modulus of elasticity	
Martensite	~ 28 GPa
Austenite	~ 83 GPa
Coefficient of thermal expansion	
Martensite	6.6 x 10^{-6}/°C
Austenite	11.0 x 10^{-6}/°C

7.1.2 shape memory polymers

SMPs are a class of active polymers which have, just like other shape memory materials, the typical shape memory effect [13]. With an external stimulus (like heat or light), SMPs can change from one shape to another shape.

SMPs do not show SME by themselves, but is fulfilled by a specific programming process. First, the permanent shape B is formed by conventional processing. Subsequently, during the programming process, the polymer is deformed and the temporary shape A is fixed. The polymer can recover to its initial permanent shape by application of an external stimulus, such as heat. SME is then observed when the polymer is heated up above a transition temperature (T_{trans}).

The molecular mechanism for inducing SME, in case of heat as an external stimulus, is shown in Figure 39. The network chains are used as molecular switches to stabilise the SMP in the deformed state. Besides the molecular switches, the elastic polymer network consist of covalent netpoints, which determine the network's permanent shape [13, 75]. The switching segments are flexible, when the temperature is higher than T_{trans}. The polymer network can then be deformed elastically. Cooling down below T_{trans} will fix the temporary shape. After heating up again, the temporary shape will recover into its permanent shape.

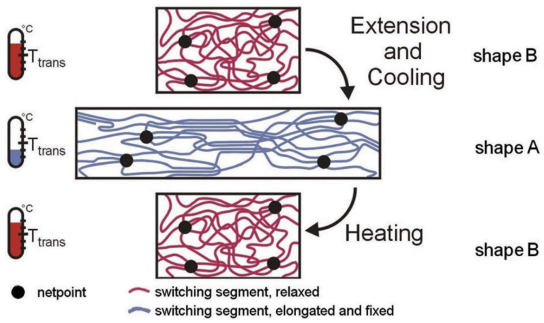

Fig. 39: Molecular mechanism to induce SME in shape memory polymers by using heat as an external stimulus. Adapted from: [13].

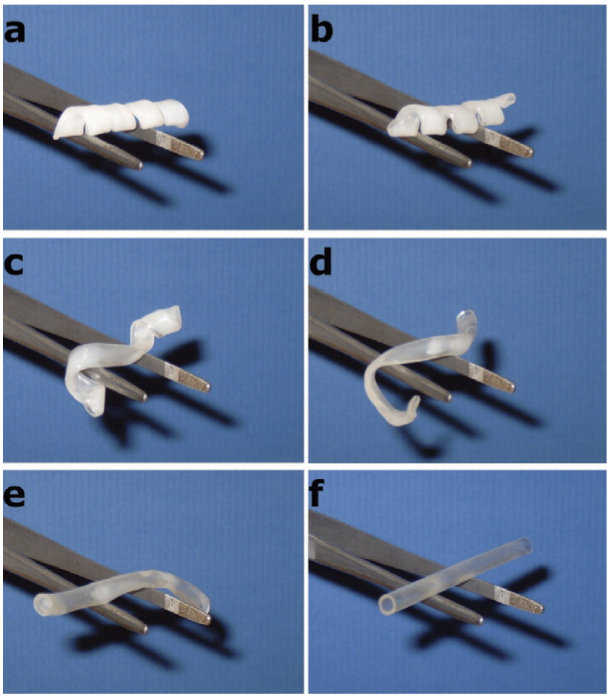

Fig. 40: Recovery of a shape-memory tube. From start (a) to finish (f), the process took 10 seconds, at a temperature of 50 °C. The polymer was programmed to form a flat helix. Reprinted from: [76].

Figure 40 shows a time series of photographs of the recovery phase of an SMP tube, which shows a thermally induced SME.

Polyurethane-based shape memory polymers

An important group of SMPs are the polyurethane-based shape memory polymers (PU-SMPs), which are also called smart memory polyurethane (SMPU). SMPUs consist two segments: relatively hard and elastic segments and flexible soft segments [77]. Variation in the ratio of soft and hard segments makes it possible to create SMPUs with various properties in elasticity and crystallisation temperature range for example.

Several SMPUs are designs for biomedical application. Examples are: cell therapy, cell manipulation, vascular stent, ocular implants and sutures. However, wide application of SMPUs is limited by its low recovery stress, modulus and stiffness [77].

Zang et. al gave a comparison between SMAs, SMPs and cardiac muscle cells, which is shown in Table 6 [78].

Table 6: Characteristics of cardiac muscle and SMA and SMP. Adapted from: [78].

Material	Stress (MPa)	Strain (%)	Strain rate (s)	Life cycles	Efficiency (%)
Cardiac muscle	0.1	>40	4	$>10^9$	>35
SMA (NiTi-wire)	>200	>5	3	$>10^5$	>3
SMP (electroactive polymer)	180	>2	>1	$>10^5$	30

7.2 Test setup

7.2.1 Pulse width modulation technique

PWM is a technique for generating an analogue signal from a digital device, like a micro controller [79]. A PWM signal consist of two important components: the duty cycle and frequency.

Duty cycle

The duty cycle defines the amount of time in which the signal is on (in high state). The duty cycle is given as a percentage of the total time of one cycle period, see Equation 7.2.

A duty cycle of 25% means for example that the signal is on for 25% of the period and off for 75% of the period. Figure 41 shows four PWM signals with different duty cycles.

$$\text{Duty cycle} = \frac{T_{\text{on}}}{T_{\text{on}} + T_{\text{off}}} \times 100\% \tag{7.2}$$

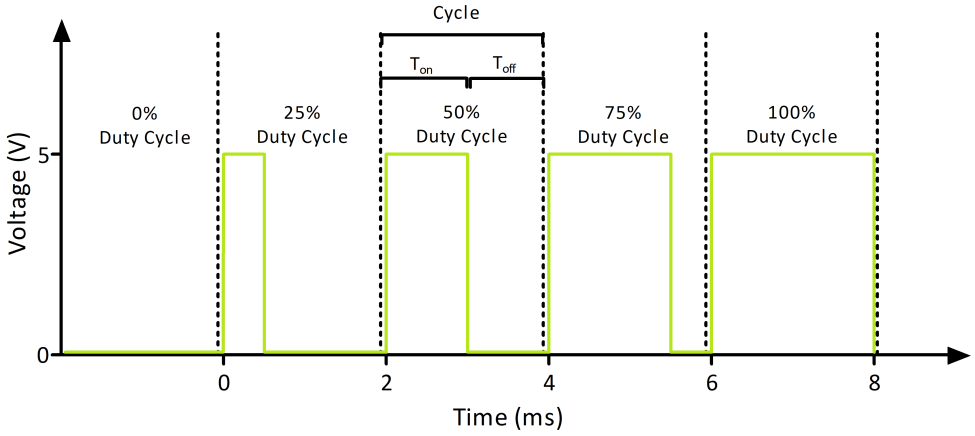

Fig. 41: Duty cycles. T_{on} is time in which the signal is on in case of a high level and T_{off} is the time of the signal in case of a low level.

Frequency

The frequency determines how fast the PWM signal completes a cycle period and therefore how fast it switches between high and low levels. Frequency can be calculated by counting the number of cycles in one second or using Equation 7.3.

$$\text{Frequency} = \frac{\text{Number of cycles}}{\text{Time in seconds}} \tag{7.3}$$

Intervals

A variable of the pulse generator which is not part of the PWM technique, but has been used in this study is the interval of passing pulses. If for example the interval variable is set to "1" every electrical pulse will actively reach the SMA-wire. While, in case of an interval of "2",

one pulse will be skipped every time. The pulse generator contains a led lamp that indicates which pulses actively pass (long flashes) and which are blocked (short flashes).

7.2.2 Measuring temperature with a thermal imaging camera

Temperature in this study was measured with a thermal imaging camera (FLIR C2). The working principle of this camera will be explained in this section.

A thermal imaging camera uses infrared radiation to create a visible image. Infrared is just as visible light part of the electromagnetic spectrum. Objects that have at least a temperature of -273.15°C transmit electromagnetic waves in the infrared part. This infrared energy can be focused onto an infrared detector of a thermal camera, which after sending the information to an infrared sensor creates a thermal image. A thermal camera has a few important specifications that influences the quality of the specific thermal camera. Three of these specifications (resolution, thermal sensitivity and accuracy) are mentioned below.

Resolution

One important specifications is the resolution of the camera. The bigger the resolution of the camera, the better the quality of the image. The FLIR C2 is an entry model of the company and has a resolution of 80 x 60 pixels, which means that it has 4800 measurement points in one image, while a more advanced thermal camera can have a resolution of 640 x 480 pixels (307.200 measurements points). Measurement of the same image, but with different resolution can cause a discrepancy in the measured temperature. A higher resolution makes a measurement therefore more accurate and will show a higher image quality.

Thermal sensitivity

The sensitivity of a thermal camera describes the smallest temperature difference which the camera can detect. The higher the thermal sensitivity, the smaller temperature difference the camera can measure. The FLIR C2 has a thermal sensitivity of 0.1 °C, while a very advanced thermal imaging camera can have a thermal sensitivity of 0.03 °C.

Accuracy

Accuracy of a thermal camera describes the margin of error of the camera. This value is mostly expressed in percentage and degree Celsius. The accuracy of the FLIR C2 is $\pm$ 2 °C or 2%, while more advanced thermal imaging cameras can have an accuracy of $\pm$ 1 °C or 1%.

Drift

It is known that thermal image cameras can display thermal drift, which can be caused by non stability of the lens and increasing temperatures of the thermal camera itself [80]. When thermal drift is observed, filtering of the signal is necessary to remove this drift. An option to remove this drift is by using a high-pass Butterworth filter, which is further explained in Appendix D, Section 9.2.

7.2.3 External pressure measurements

To get more insight in pressure in the heart model during the stimulation of the SMA, an external pressure sensor was fabricated. A TAVI-balloon, which normally is used during transcatheter aortic valve implantation, was placed in the closed heart model and connected to an intravenous blood pressure sensor (501669001, Merit OEM, Maastricht) and a microcontroller to interpret pressure values on a computer.

The Meritrans pressure sensor is an external sensor which is used in combination with fluid-filled catheters. The sensor contains resistors which are bonded to a diaphragm. When pressure is applied, the diaphragm deforms and stresses one or both resistors. Changes in resistance can be converted into voltage signals by using a Wheatstone bridge circuit. Figure 42 shows an example of a strain-gage pressure sensor and the Wheatstone bridge [81]. This Wheatstone bridge consist of four active elements: R_1, R_2, R_3, and R_4. Furthermore, R_y is a resistor, R_x a potentiometer, v_i the applied voltage, Δv_0 the output voltage on a voltmeter and R_i the internal resistance. Δv_0 is zero (balanced bridge) when R_1 / R_2 = R_4 /R_3, according to the voltage-divider approach.

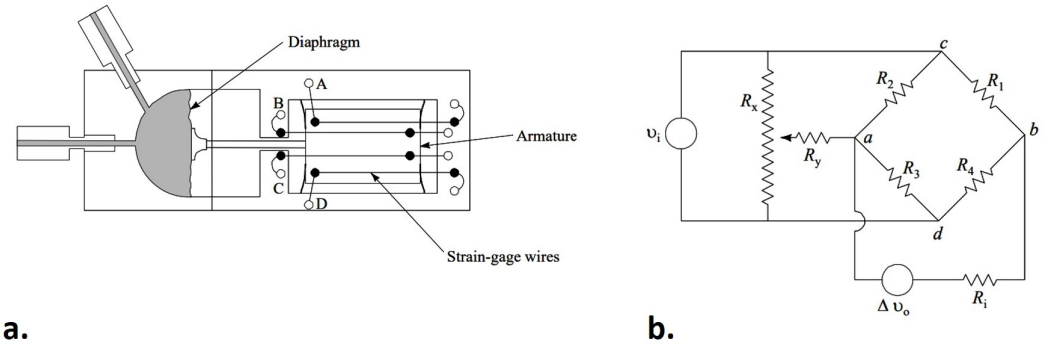

Fig. 42: Wheatstone bridge. Wher R_y = resistor, R_x = potentiometer, v_i = applied voltage, Δv_0 = output voltage on a voltmeter and R_i = internal resistance. Adapted from: [81].

A resistance-form sensor can be connected in one or more arms of the Wheatstone bridge circuit. Measuring Δv_0 with an amplifier which is connected to and analogue-to-digital converter (which in turn is connected to a computer), makes it possible to detect variation in resistance and therefore to measure pressure.

Assumed that all values of resistance of the Wheatstone bridge are equal to R_0 initially, and $R_0 \ll R_1$, an increase in resistance (ΔR), for all resistances will still lead to a balanced bridge. However, if for example an increase in R_1 and R_3, and decrease in R_2 and R_4 , by ΔR, then Δv_0 can be calculated with:

$$\Delta v_0 = \frac{\Delta R}{R_0} \cdot v_i \tag{7.4}$$

The output voltages of the sensor can be calibrated by applying known pressures on the diaphragm and record the output voltages.

Calibration

The pressure sensor has to be calibrated to match the voltage values to the measured pressure. Calibration was performed by measuring voltages at known pressures of 0, 10, 20 and 30 psi. The calibration curve is presented in Figure 43. With a r^2 of 1 is this curve perfect linear and useful to convert measured voltages to specific pressures.

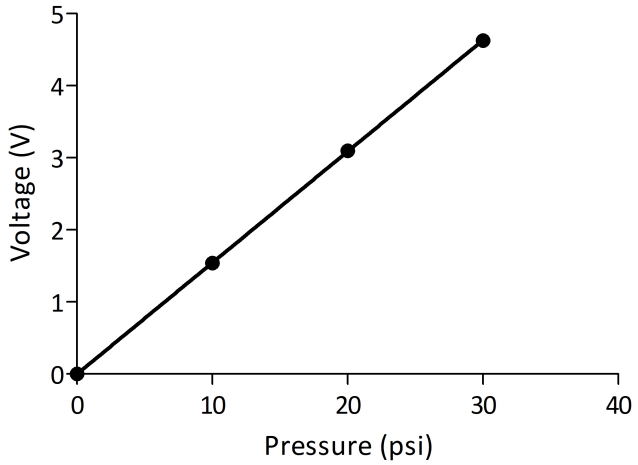

Fig. 43: Calibration curve of pressure sensor.

The used microcontroller, an Arduino Uno, consist of a 10 bit analogue to digital converter. This means that it has the ability to detect 2^{10}(=1024) values. Because measurements are between a range of 0 - 5 V, the resolution of this microcontroller is $\frac{5\,\text{V}}{1024} = 0.00488\,\text{V}$.

The formula of the calibration curve is:

$$V = 0.1544P + 10^{-5}$$

The smallest measurable increase in pressure is therefore:

$$P = 0.00487 \cdot \frac{1}{0.1544} = 0.03236..\ \text{psi} \approx 1.63\ \text{mmHg}$$

7.3 Review of power supply of pacemakers and mechanical devices

7.3.1 Electric Power

Electric energy can be easily transformed into other forms of energy. A motor for example, transform electric energy into mechanical energy. Electric power is the rate at which electric energy of a device is transferred. Electric power can be calculated with Equation 7.5, in which P is electric power, I is current which is passing through the device and V is the potential difference across it.

$$P = I \cdot V \tag{7.5}$$

The SI unit of P is the watt, and 1 watt is equal to 1 J/s.

Electric power is not the same as the total used energy of a device. Power is the rate of energy transformation, so the total energy which is used by a device can be calculated by multiplying the power consumption by the time at which the device is on [82]. A frequently used unit for specifying the energy, is the kilowatt-hour (kWh). One kWh = (1000 W)(3600 s) = 3.6 x 10^6 J.

7.3.2 Pacemaker (regular and CRT)

Most pacemaker batteries have a capacity between 1 and 2 Ah, while ICDs have a somewhat higher capacity between 1.5 and 2.5 Ah [27]. The current for a dual-chamber pacemaker, which paces at 60 pulses/min with conventional voltage and normal impedance leads, will range between 3 and 10 μA. The longevity of pacemaker battery can be calculated by dividing the current through the capacity of the battery.

A pacemaker which consumes for example 15 μA (in which the energy consumption for data logging is included) and has a battery capacity of 1.2 Ah (1.2 x 10^6 μAh) has a longevity of:

$$\frac{1.2 \cdot 10^6}{15\ \mu\text{A}} = 80,0000 \text{ hours} = 9 \text{ years}.$$

The power supply of ICDs is not the same as the power supply of pacemakers because of their difference in energy demands. A pacemaker delivers low energy pacing impulses, typically with 10 to 15 μJ, while an ICD must be able to give a shock of up to 40 J.

7.3.3 Left ventricular assist device

The power consumption for different LVADs are shown in Figure 44 [83–86]. A constant power delivery is extremely important for a LVAD, since a loss of power will stop the pump of th LVAD, with severe consequences.

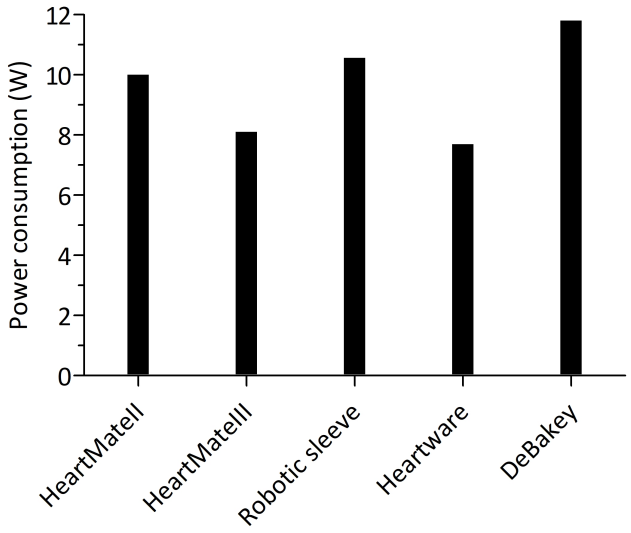

Fig. 44: Power consumption of different LVAD systems [83–86].

The constant demand for power makes it crucial for patients to replace the batteries in time. Besides the use of batteries, implanted pump of the LVADs can be connected to an external power source, such as a power module which delivers alternating current electrical power. In case of the HeartMate II, the power source of the pump consist of an external power module or a pair of lithium ion batteries. These two batteries of 14 V (4.8 Ah, 71 Wh) makes it able to run the LVAD for minimal six hours, in nominal use [87]. This means that the HeartMate II consumes 23.7 Watt-hour (142 Wh/6).

8 Appendix C: Design phase

8.1 Problem analysis and requirements

The design process starts by analysing the problem and making a list of requirements and wishes for a possible solution.

As mentioned in the introduction (see Chapter 1), HF is a clinical syndrome with unpleasant symptoms such as dyspnoea, tiredness and oedema [1]. HF is increasingly prevalent in West-European countries and purposes of treatment in patient with HF are to improve their clinical condition, quality of life and functional capacity, prevent hospital admission and reduce mortality. Despite optimal medical treatment, many patients still remain symptoms. A select group of HF patients are eligible for treatment with CRT, which should improve refilling and contraction pattern of both ventricles. However, 30 - 40 % of the patients who are treated with CRT remain non-responders [9]. In case of end-stage HF, left ventricular remodeling surgery or implantation of a LVAD can serve as a bridge to heart transplantation. These interventions are invasive for patients and usually only desirable in a late stadium of HF. Due to limitations of CRT, LVADs and heart transplantation, it is desirable to develop a new resynchronisation therapy in which all patients with HFrEF are eligible for treatment.

A new resynchronisation device should fulfill some important requirements and preferably also a number of wishes. The requirements were divided into four different categories: user requirements, safety requirements, ergonomic requirements and durability requirements. Furthermore, a list of wishes for the device were formulated.

User requirements

The device should:

1. Allow counterclockwise rotation of the left ventricle apex during systole [18];
2. Not oppose the clockwise rotation (untwisting) of the left ventricle apex during the isovolumic relaxation and early period of diastole [18];
3. Be able to displace additional volume;
4. Be electrically paced synchronously with ventricular systole and therefore be able to sense the cardiac P or R wave [88];
5. Be implantable within 3 hours;
6. Support the heart for at least every 5th heartbeat;
7. Be activated during systole and de-activated during diastole.

Safety requirements

8. The device should not damage the heart or surrounding tissue:
    a) The device should be biocompatible [12];
    b) The device should not have sharp edges;
    c) The device should not be too warm (maximum heat flux of 40 mW/cm^2) [89].

Ergonomic requirements

9. The shape of the device should fit in the patients body;
    a) Depending on the sort of device, endocardial or epicardial, the device should fit in the left ventricle or space around the heart, respectively.
10. The device should have a minimum durability of five years.

Whishes

1. Minimal invasive implantation of the device;
2. Easy implantation of the device;
3. The device should be MRI proof;
4. No need for intake of anticoagulation.

8.2 Function analysis

After formulating the requirements and wishes of the new device, the desired function of the new device was analysed. A main function should be described with two abstract words. One word has to be selected out of: material, energy or information. And the other word has to be selected out of: transportation, transformation, storage, separation or combination.

In the case of a device which could support the human heart to increase EF, the main function can be described as "Transport material (blood)".

This main function can be divided into multiple subfunctions. These subfunctions are described on the same way as the description of the main function. Figure 45 shows the subfunctions over time to support the heart and to make it possible to pump additional blood from the heart to the rest of the body. First of all, a smart material should be attached to the epicardium and/or endocardium (1. Material storage). Secondly, energy should be delivered to the smart material to be able to deform its shape. An SMA is able to deform its shape when it is heated by a current (2. Energy transportation). Thirdly, the smart material can be used in different combinations, to create the desired displacement of the ventricle wall (3. Material combination). Fourthly, the smart material should be in a form which makes it able to create forces by the displacement of the material (4. Material transformation). At last, the device should be able to pump an additional amount of blood through the aorta, which is the main function of the device (5. Material transport).

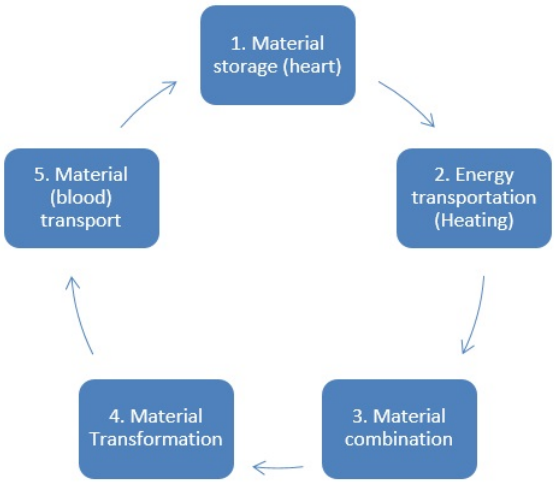

Fig. 45: Function block scheme of a heart support device.

8.3 Synthesis

The next step in the designing phase was to collect multiple solutions for the different subfunctions in one morphologic scheme, see Figure 46. Different pre-concepts were created from this morphologic scheme, by selecting one solution from each row. Each path through that scheme resulted in a pre-concept, which in total has lead to ten pre-concepts.

Function\ Solution	1.	2.	3.	4.	5.
a. Material storage (attachment to the heart)	Glue	Anchor	Screw	Sutures	
b. Energy transportation (current delivery)	Pacemaker+leads	External battery	Kinetic energy		
c. Material combination	Single wire	Bundled wires	Spring	Spring with wires	Woven wires
d. Material transformation (force creation)	Belt	Spiral	Helical form	Patch	Net
e. Material transport	Pull	Clamp	Push	Pressure	

Fig. 46: Morphologic scheme.

Table 7: Composition of pre-concepts, based on morphologic scheme.

	Nr	Material Storage	Energy transportation	Material combination	Material transformation	Material transport
Pre-concept	1	A1/A4	B1/B2	C2	D1	E3
	2	A1/A4	B1/B2	C1	D2	E3
	3	A1/A4	B1/B2	C2	D1	E3
	4	A1	B1/B2	C1	D1	E3
	5	A1/A4	B1/B2	C	D	E
	6	A1/A4	B1/B2	C4	D1	E2
	7	A4	B1/B2	C1/C3	D5	E4
	8	A2/A3	B1/B2	C3	-	E1
	9	A1/A4	B1/B2	C5	D1	E1
	10	A1/A3	B1'B2	C5	D4	E3

8.3.1 Pre-concepts

The pre-concepts were selected by selecting one solution from each row. The composition of the selected solutions for the different pre-concepts is showed in Table 7. Each pre-concept is visualised and explained shortly in this section.

Pre-concept 1: Circular band

This pre-concept consist of a bundle of multiple single SMA wires, which are wrapped around the heart in shape of a band, see Figure 47. Activation of SMA wires will compress the heart layers in a circumferential way and lead to an additional flow from the ventricle towards the aorta.

Pre-concept 2: Spiral

This pre-concept consist of one single SMA wire, which is widely wrapped in a spiral shape around the heart, see Figure 48. In this design, a big part of the heart underwent an additional compression when the SMA wire is stimulated.

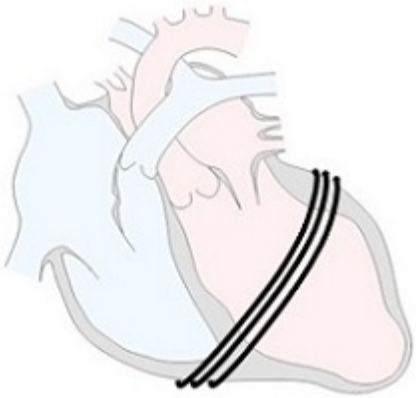

Fig. 47: Concept 1: Circular band.

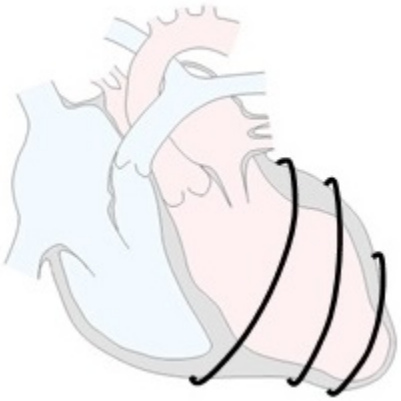

Fig. 48: Concept 2: Spiral.

Pre-concept 3: Oblique band

This pre-concept consist, just like the first pre-concept, of multiple single wires in a band shape. However, this band has an oblique direction, which in theory compresses the heart in more longitudinal direction, see Figure 49.

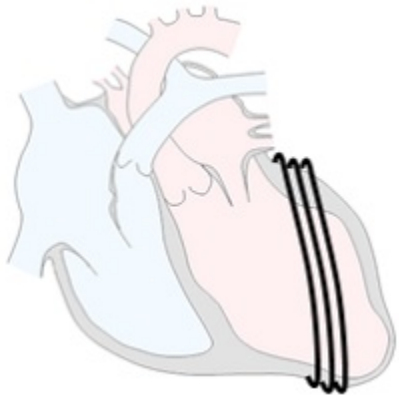

Fig. 49: Concept 3: Oblique band.

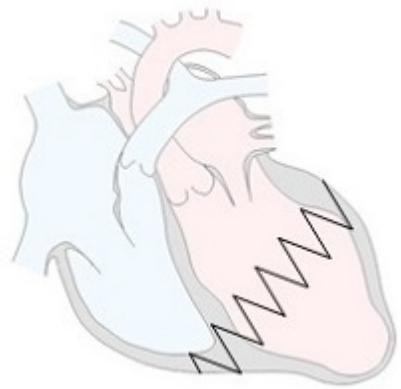

Fig. 50: Concept 4: Zigzag band.

Pre-concept 4: Zigzag band

The zigzag pre-concept is a design of a single wire, which follows a line with small corners between two imaginary parallel lines, and surrounds the heart, see Figure 50.

Pre-concept 5: Cross

This pre-concept is a combination of the circular band and an oblique SMA wire, see Figure 51. This design reflects the two layers of the heart, which are responsible for the contraction of the heart.

Pre-concept 6: Spring construction

In contrast to the previously described pre-concepts, this pre-concept focuses on helical springs made of an SMA, see Figure 52. A great advantage of a spring is the large deformation possibility.

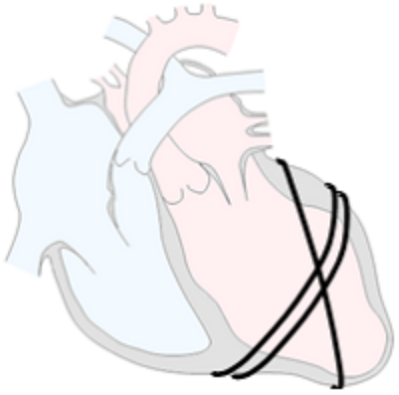

Fig. 51: Concept 5: Cross.

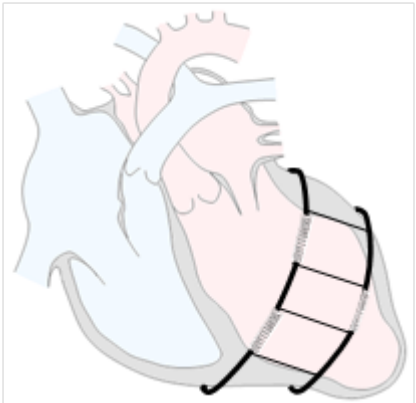

Fig. 52: Concept 6: Spring construction.

Pre-concept 7: Net

This pre-concept consist of a passive net, which fits snuggly around the heart and therefore prevents further dilatation, see Figure 53. This net can be made active, by placing smart materials (wires or springs) between two ends of the net, which makes it possible to tighten the net. This will cause a mechanical pressure on the heart during systole.

Pre-concept 8: Endocardial spring

This pre-concept consist of one or two springs in the LV, see Figure 54. The idea is that two springs can pull the ventricular walls together, and therefore will displace additional volume.

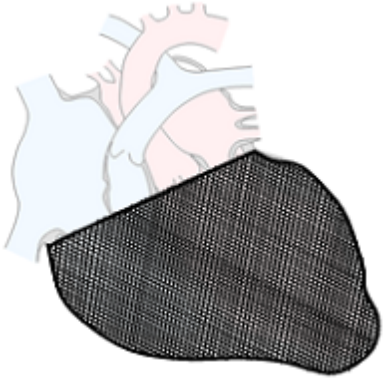

Fig. 53: Concept 7: Net.

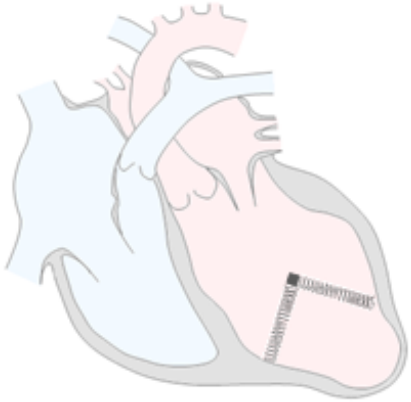

Fig. 54: Concept 8: Endocardial spring.

Pre-concept 9: Woven band

This pre-concept looks like pre-concept 1, the band-shape. However, this pre-concept consist next to horizontal SMA-wires also vertical or oblique SMA-wires, which makes it possible to pull the outer horizontal wires to each other, see Figure 55.

Pre-concept 10: Patch

A totally different pre-concept is the patch. The patch is a kind of plaster in which SMA-wires can be placed in random directions, see Figure 56. One or multiple patches can for example be placed at specific parts of the heart which have a disrupted wall movement.

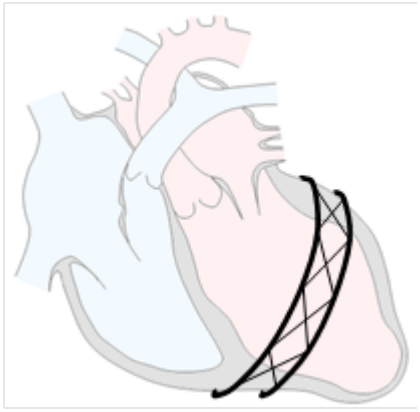

Fig. 55: Concept 9: Woven band.

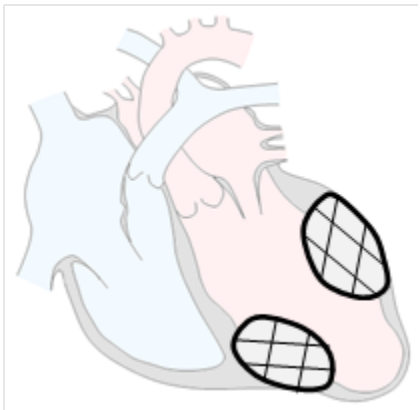

Fig. 56: Concept 10: Patch.

8.3.2 Concept selection

To select the best pre-concepts, each pre-concept was reviewed based on the earlier defined requirements. Each requirement was given a score (1 to 10) with respect to its importance. Subsequently, the pre-concepts were scored (1 to 10) based on how they fulfills each requirement. This score was multiplied with the importance score of the requirement, for each requirement. Thereafter, the scores for every requirement were summed up for every pre-concept, see Table 8. The best pre-concepts, selected from this table, were: the circular band, the spiral, the oblique band and the cross shape.

Table 8: Concept selection

Requirement	WF	1	2	3	4	5	6	7	8	9	10
Allow rotation left ventricle	7	8	7	7	7	7	7	6	10	8	9
Fast implantation	6	6	5	5	5	5	5	5	3	5	6
Displace additional volume	9	6	8	7	5	9	7	6	5	6	5
Not damage surrounding tissue	8	9	8	8	8	8	7	7	5	8	7
Should fit in human body	5	9	8	8	8	8	8	8	9	8	9
Durability of minimal five years	5	7	7	7	7	7	7	6	5	7	7
Total		**298**	**290**	**281**	263	**299**	273	252	243	279	280

9 Appendix D: Protocols

9.1 Test setup and determination of volume displacement

The necessary materials for determining the volume displacement are:

- A paediatric ventilation balloon (that serves as a static heart model);
- Tube that fits in the ventilation balloon;
- Demineralised water to fill the balloon and the tube (partly);
- A tripod and clamps to fixate the ventilation balloon;
- A tape measure;
- Shape memory alloys;
- Cable shoe connectors, screw terminals, vascular ties and velcro straps for securing the shape memory alloy;
- Power supply, pulse generator and power cables;
- Compact camera on tripod.

Fig. 57: Test setup.

The necessary steps for measuring the volume displacement are as follows:

1. Attach the ventilation balloon and tube to tripod with clamps and cable ties (see Figure 57);
2. Fill ventilation balloon completely with demineralised water and make sure that water level in the tube is as high as the top of the water-filled balloon and there are no air bubbles left;
3. Connect the ends of the SMA-wire(s) with small power cables by using cable shoe connectors;
4. Position the SMA-wire(s) in the desired shape around the ventilation balloon behind the vascular ties;
5. Attach the SMA-wire ends to screw terminals by using a screwdriver;

6. In case of multiple SMA-wires, be sure that small power cables are connected in the right way to make a parallel or series circuit;
7. Connect small power cables with power supply and pulse generator, as was shown in Figure 5;
8. Set the desired frequency, duty cycle and interval of the electrical pulses from the pulse generator;
9. Put the camera on a tripod and film the fluctuating water level in the tube;
10. Load movie in Kinovea software, start Track Path and move the video forward. Tracking is a semi-automatic process in Kinovea. The points location is computed automatically but you can adjust them at any time if necessary;
11. Convert the measured displaced centimeters into displaced milliliters and load data into Graphpad Prism to make graphs.

The technical specifications of Dynalloy's Flexinol® can be found in Table 9.

Table 9: Specifications of Flexinol ®

Diameter (mm)	Resistance (Ω/m)	Heating pull force (grams)	Current for contraction (mA)
0.15	55	321	410
0.25	18.5	891	1050
0.38	8.3	2250	2250

9.2 Determination of temperature fluctuations with a thermal camera

Materials

The used materials for determination of temperature fluctuations during activation of the SMA are:

- Setup with the ventilation balloon (as described in Section 9.1);
- FLIR C2 thermal camera (FLIR Systems, Wilsonville, Oregon, USA), as shown in Figure 58;
- Additional tripod and clamp;
- Computer with FLIR Tools software.

Fig. 58: FLIR C2 thermal camera.

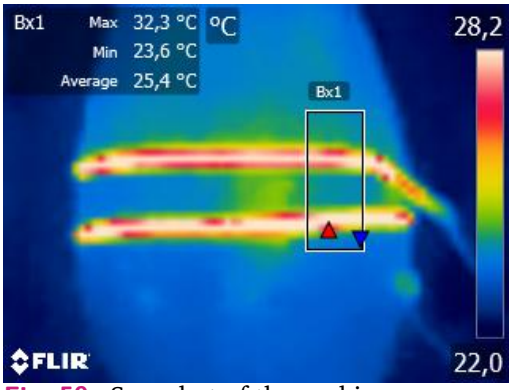

Fig. 59: Snapshot of thermal image video.

Preparation and performing of thermal experiments

The necessary steps for measuring temperature fluctuation are as follows:

1. Make sure that the thermal camera is fully charged;
2. Connect and fixate SMA-wires as described in Section 9.1;
3. Set the thermal camera in "thermal modus";
4. Focus the thermal camera;
5. Connect the USB cable of the camera to a computer;
6. Start FLIR Tools software;
7. Add one or more box measurements to thermal image, to measure minimal and maximal temperature within this box, see Figure 59;
8. Stop measurement and save data from the measurement box.

Analysing of data

As mentioned before, the thermal camera showed some linear drift during the measurement. This made it necessary to filter the raw data before the data could be analysed. Matlab R2016b (MathWorks, MA) was used to filter the linear drift, by using a high-pass Butterworth filter. The created Matlab script is shown in Figure 60. The results of the application of a high-pass Butterworth filter is shown in Figure 61.

```
clear all;
close all;

load('D:\Programmas\Matlab M3\Tempmeasure.mat') %Load data

figure(1)
plot(Time,Temp)

%% Define time periods
Temp1 = Temp(1649:1945);
Time1 = Time(1649:1945);
Temp2 = Temp(1946:12371);
Time2 = Time(1946:12371);
Time3 = [Time1;Time2];


%% Make Fast-Fourier transformation plot
fs=3.75; %Sample frequency
Ts=1/fs; %Sample time
M=2^11;
f=(0:(M-1))/M*fs;
xhat=Ts*fft(Temp2,M);

figure(2)
plot(f(1:M/2),abs(xhat(1:M/2)))

%% Use high-pass Butterworth filter
fc=0.01;  % Cut-off frequency
nfc=fc/(fs/2);

[B,A]=butter(4,nfc,'high'); %fourth-order high-pass Butterworth
filter

y1=filtfilt(B,A,Temp2);

figure(3)
plot(Time2,y1+31.3) %correct for removed off-set
ylim([0 40])
```

Fig. 60: Matlab script for filtering raw data of thermal image camera. Performed with Matlab R2016b.

The red en green horizontal line in Figure 61 represents the mean of the maximal and minimal measured temperature, respectively. These lines were created by using Matlab's function "findpeaks", which is shown in Figure 62. The two lines shows that temperature stayed stable for the time of the measurement.

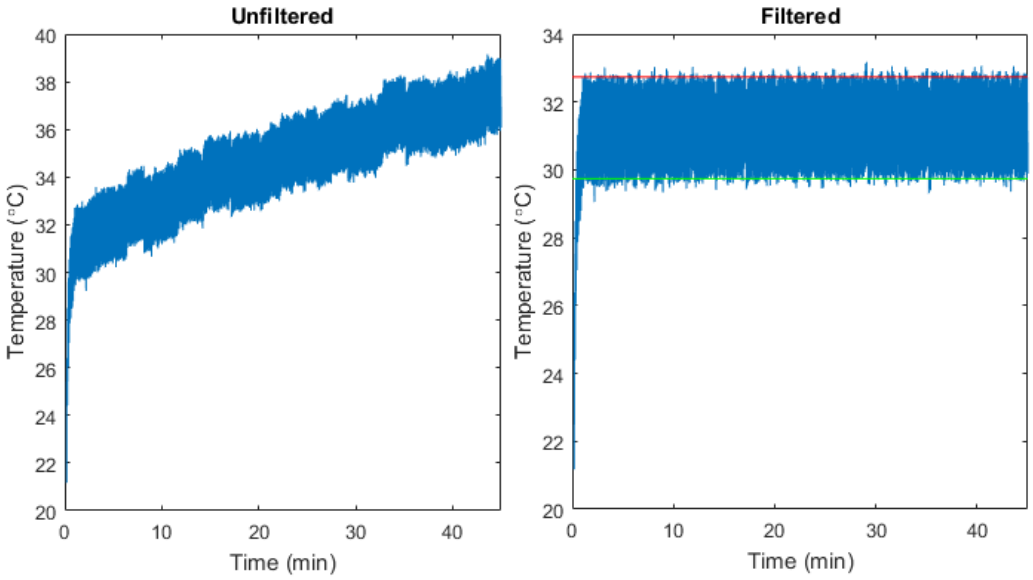

Fig. 61: Results of temperature data. Left figure shows the raw data before filtering and right figure shows the result after filtering. Bigger differences in temperature as seen in the left figure were caused by automatic calibration of the thermal camera.

```
%% Find peaks for adding reference line

y2=y1+31.3;

figure
findpeaks(y2,fs,'MinPeakHeight',32.3,'MinPeakDistance',4.5);
[Maxima,MaxIdx]=findpeaks(y2,fs,'MinPeakHeight',32.3,'MinPeakDistance',4.5);
mean_maxvalue= mean(Maxima)
DataInv =  -y2;

figure
findpeaks(DataInv,fs,'MinPeakHeight',-30.2,'MinPeakDistance',4.3);
[Minima,MinIdx]=findpeaks(DataInv,fs,'MinPeakHeight',-
30.2,'MinPeakDistance',4.3);
Minimas = -Minima;
mean_minvalue=mean(Minimas)

figure
plot(Time3,Temp3)
hold on
hline2=refline(0,mean_maxvalue)
hline2.Color='r';
hold on
hline3=refline(0,mean_minvalue)
hline3.Color='g';
```

Fig. 62: Matlab script for finding minimal and maximal temperature peaks.

9.3 Determination of pressure build-up within ventilation balloon

The used materials for determination of the pressure within the ventilation balloon are:

- Setup with the ventilation balloon (as described in Section 9.1);
- A stopper to stop the opening of the ventilation balloon;
- TAVI-balloon;
- Hand pump with pressure gauge;
- External pressure sensor;
- Amplifier;
- Microcontroller;
- Laptop with Matlab software.

The necessary steps for measuring pressure are as follows:

1. Use setup with the ventilation balloon (as described in Section 9.1), but remove tube at the bottom and use a stopper to stop this opening of the ventilation balloon;
2. The opening at the upper side of the balloon should be covered with a rubber ring, to prevent water leakage;
3. Fill TAVI-balloon with demineralised water by using the hand pump. Be sure that all no air bubbles are left in the system, because air is easier to compress than water and can therefore affect the measurement;
4. Place TAVI-balloon in the ventilation balloon;
5. Connect pressure sensor to amplifier and microcontroller, which in turn should be connected to a laptop (see Figure 63);
6. Run the first commands of the Matlab script, as shown in Figure 64;
7. Perform calibration measurements by applying pressure to TAVI-balloon (pressure can be read from pressure gauge of hand pump) and read out voltage value from pressure sensor;
8. Enter calibration values in Matlab script;
9. Activate SMA-wires with power supply and pulse generator and measure pressure by running the remaining commands of Matlab script (see Figure 64);
10. The choppy raw data can be saved and filtered by using the Matlab script (see Figure 65);
11. Pressure can be read from the resulting graphs.

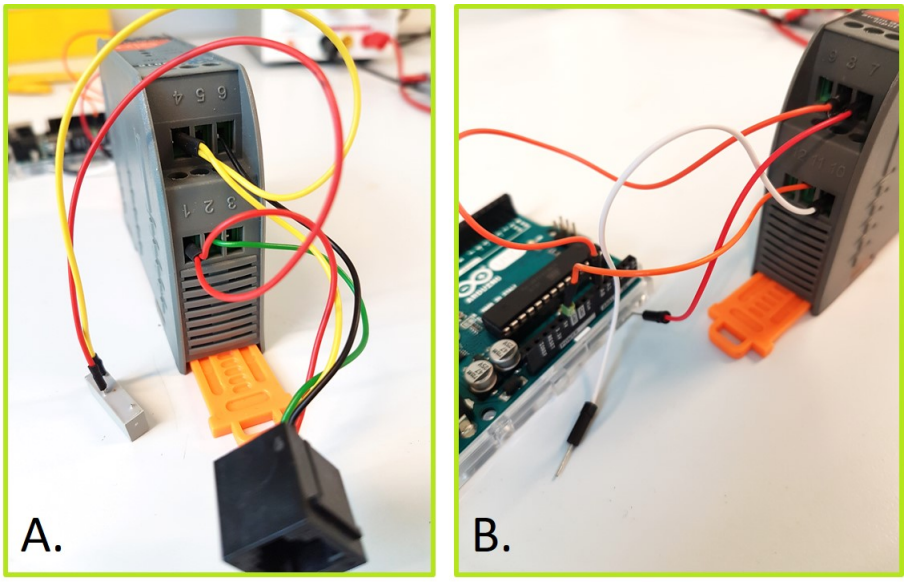

Fig. 63: Connection of sensor to microcontroller. A. Connection of sensor connection point to amplifier. B. Connection of amplifier to microcontroller.

```
clear all
close all

%% Connect to arduino
a = arduino ('COM5', 'UNO') %type in COM-port and type of Arduino

%% Read voltage on A0 Arduino pin
v = readVoltage(a,'A0')

%% Record and plot 100 seconds of pressure data using polyfit
clear all, close all, clc
ii=0;
pressure=zeros(1e4,1);
pressure2=zeros(1e4,1);
t=zeros(1e4, 1);
a = arduino ('COM5', 'UNO');

%% Fill in calibration values
calib_pressure=[0 10 20 30]; %in psi
calib_V=[0 1.5396 3.0987 4.6285]; % in V
P1=polyfit(calib_V, calib_pressure,2);

%% measure voltage output for certain amount of time and fit it (with
polyval) to the calibration

tic  %tic = start stopwatch timer
while toc<100  %100 seconds
    ii=ii+1;
 %read current pressure value
    v=readVoltage(a,'A0');
 %calculate pressure from voltage (based on calibration function
or polyfit)
    pressure(ii)=(polyval(P1,v))-P1(3); % in psi
    pressure2(ii)=(v*6.47668)-0,00001; %in psi
    t(ii)=toc;
End
```

Fig. 64: Matlab script to read out voltage values from pressure and conversion to pressure values.

```
%% Post processing of data
pressure = pressure(1:ii); %remove any excess zero's
pressure2=pressure2(1:ii);
pressure_mmHg=pressure*51.71;   %convert to mmHg
pressure2_mmHg=pressure2*51.71; %convert to mmHg
t = t(1:ii); %remove any excess zero's

figure(2);
plot(t,pressure_mmHg,'r') %plot data
hold on
plot(t,pressure2_mmHg,'b')
xlabel('time (sec)')
ylabel('pressure (mmHg)')
title('Pressure data')
legend('Polyfit calibration','linear formula calibration')
set(gca,'xlim',[t(1) t(ii)])

figure(3);
plot(t,pressure_mmHg,'r')
xlabel('time (sec)')
ylabel('pressure (mmHg)')
title('pressure data')

%% Export data to Excel file
pressureresults =
table(t,pressure_mmHg,pressure2_mmHg,'VariableNames',{'Time_sec',
'Pressure_mmHg','pressure2_mmHg'});
filename = 'pressure_measurement1.xlsx';

writetable(pressureresults,filename)

%% Filtering signal with Moving Average (MA) filter
B = 1/20*ones(10,1);
out = filtfilt(B,1,pressure_mmHg);

figure(4);
plot(t,out)
```

Fig. 65: Matlab script to save and filter the raw data.

Appendix E: Additional graphs

10

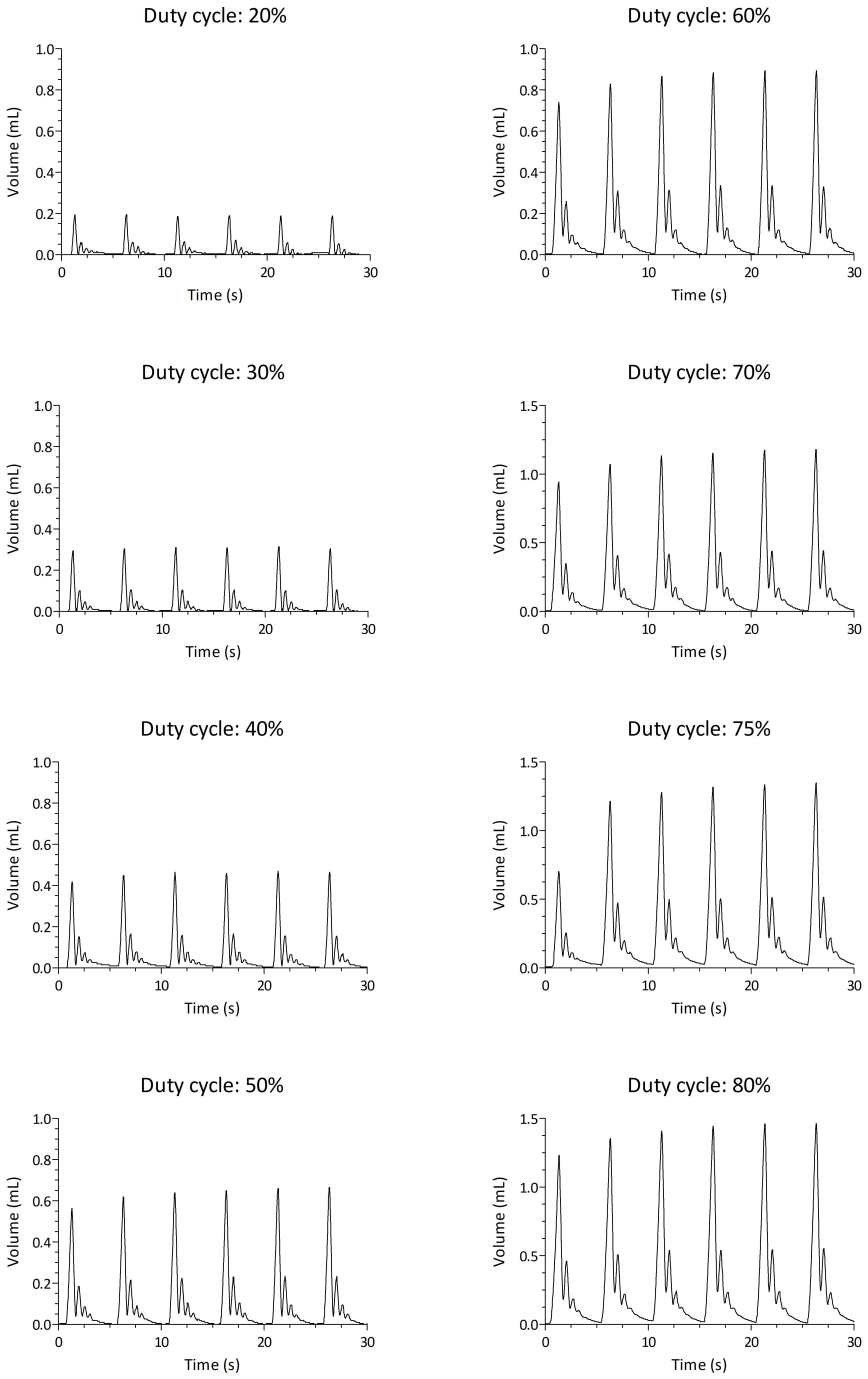

Fig. 66: Volume displacement for different duty cycles.

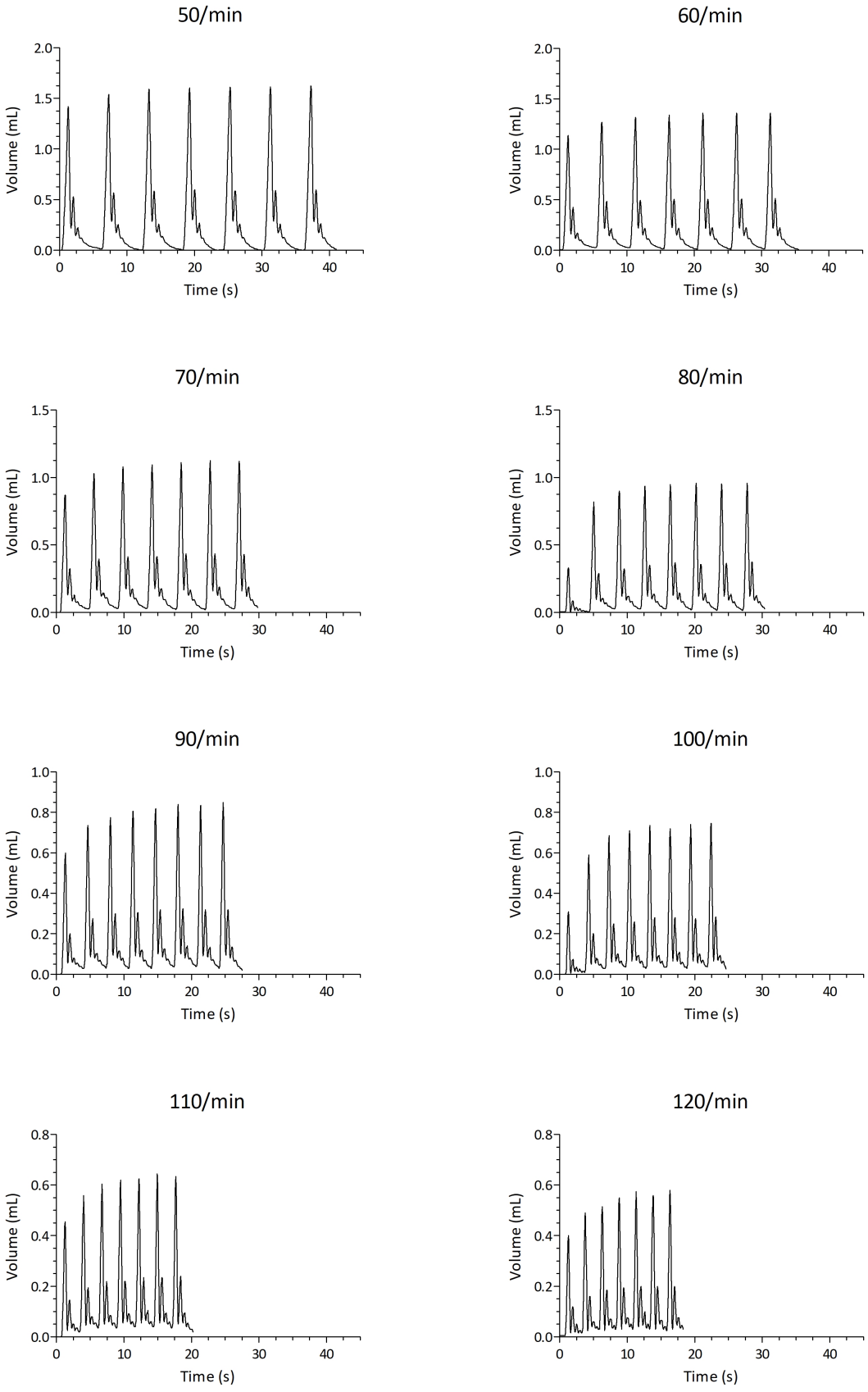

Fig. 67: Volume displacement for different frequencies.

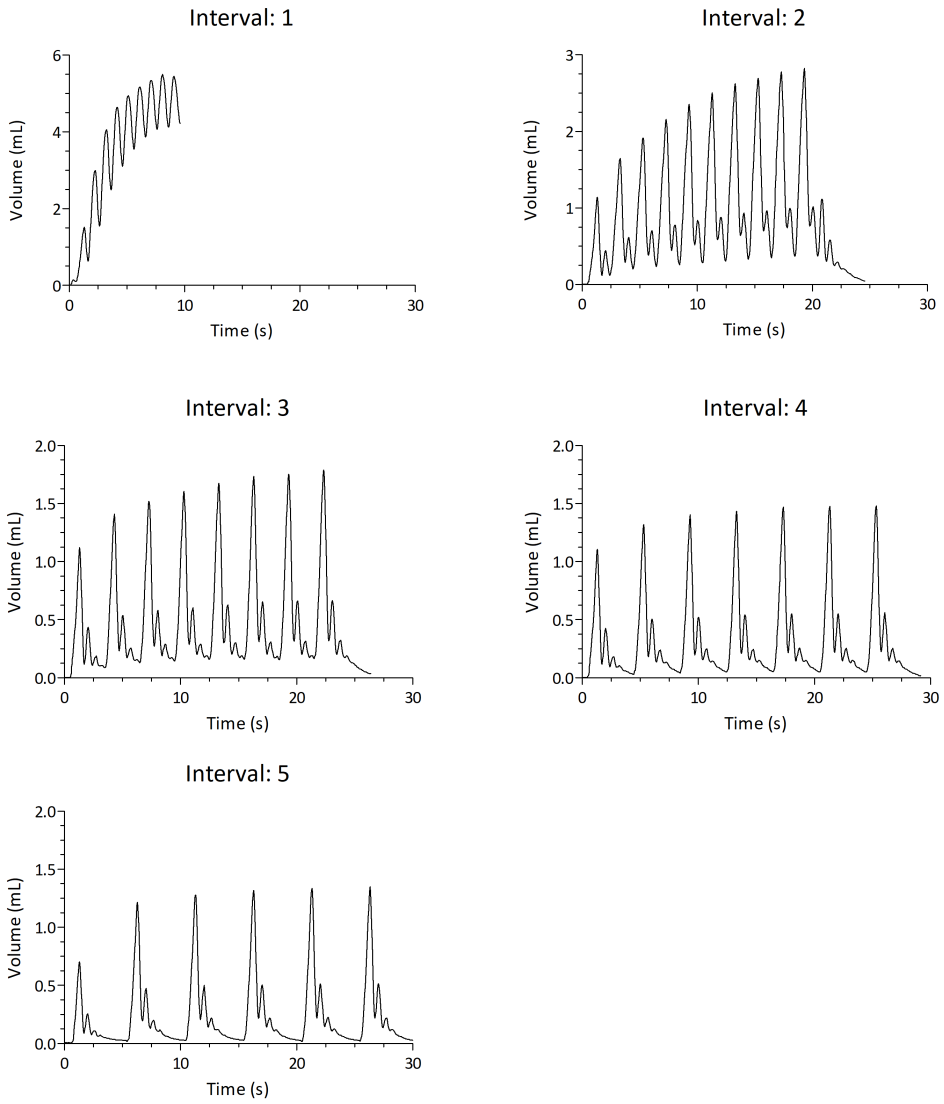

Fig. 68: Volume displacement for different pulse intervals.

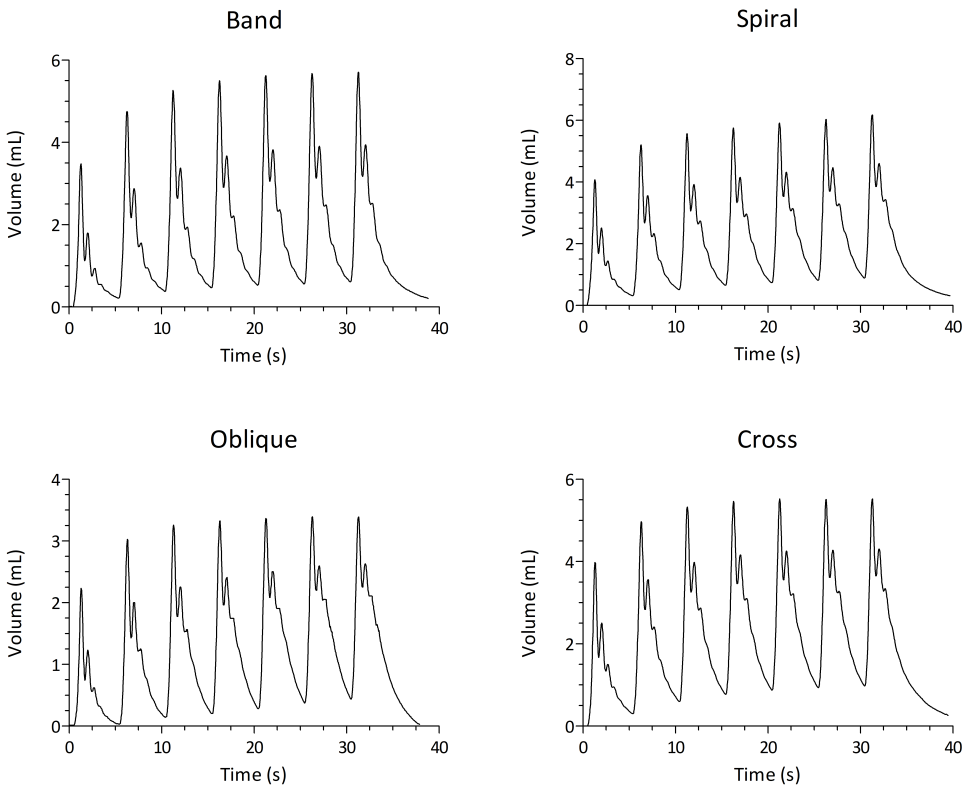

Fig. 69: Volume displacement for different designs.

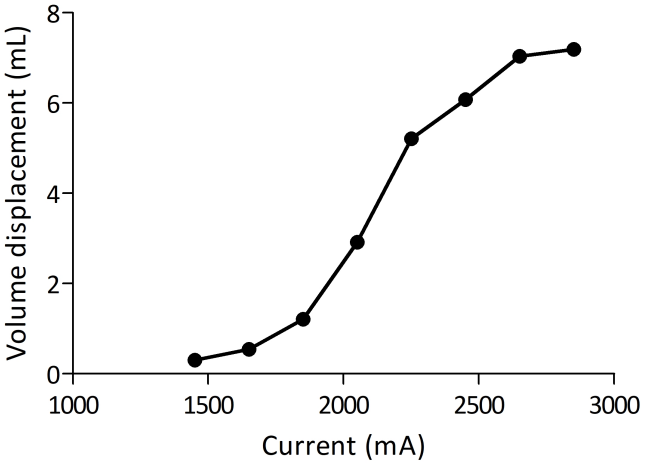

Fig. 70: Influence of current on volume displacement. Each point represents the maximal achieved volume out of five activation pulses.

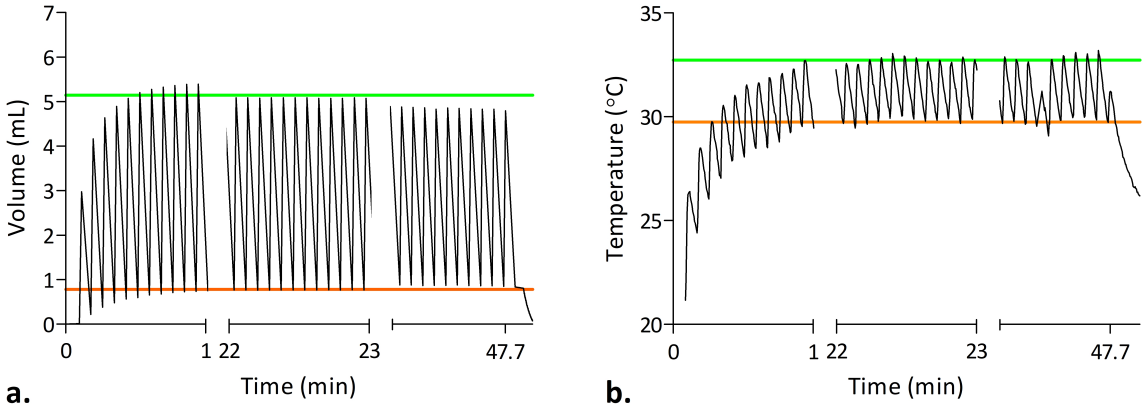

Fig. 71: Long-term measurement. One SMA-wire was disconnected from screw terminal, causing a decreasing volume displacement (a) and finally a disconnected current circuit, which can be seen as an immediately decrease in temperature (b).

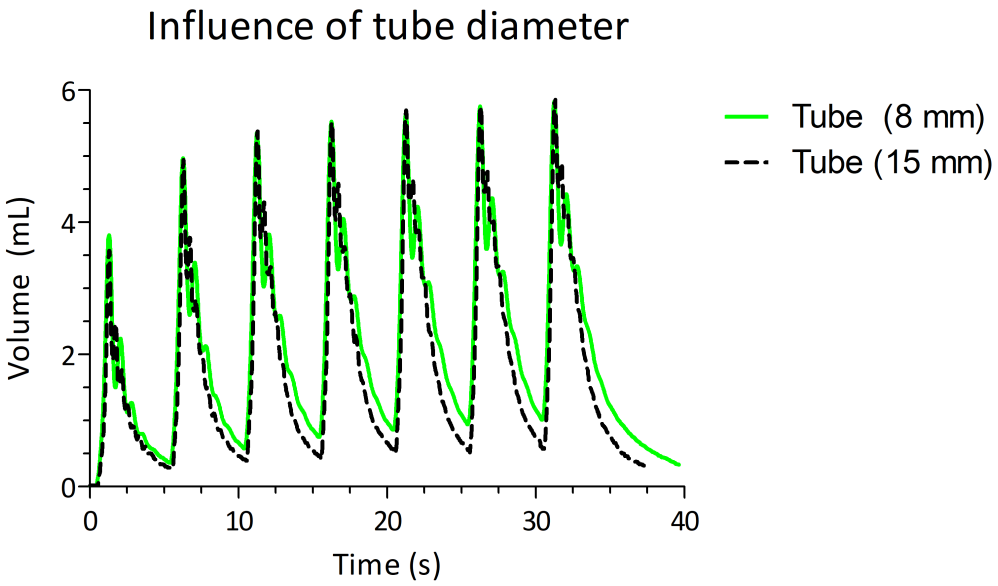

Fig. 72: Volume displacement for two different sizes of tube diameter.

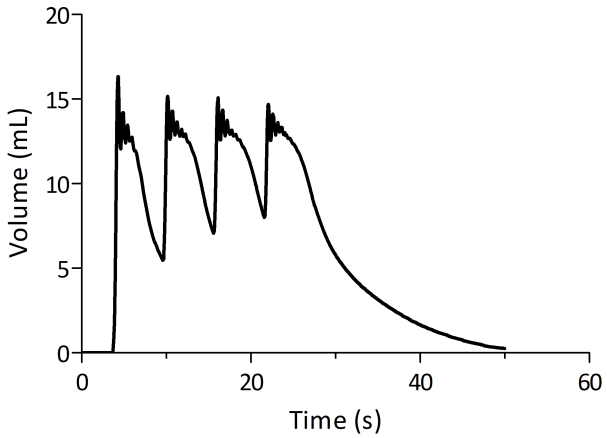

Fig. 73: Volume displacement of measurement with rings.

Fig. 74: Picture of the used rings to distribute force to heart model.

References

1. Rutten, F. H., Walma, E. P., Kruizinga, G. I., Bakx, H. C. A. & Van Lieshout, J. in *NHG-Standaarden 2009* 193–212 (Springer, 2009) (cit. on pp. 1, 54).
2. American Heart Association. Nomenclature and criteria for diagnosis of diseases of the heart and great vessels. *New York: Little Brown & Co* (1994) (cit. on p. 1).
3. Hunt, S. A. ACC/AHA 2005 guideline update for the diagnosis and management of chronic heart failure in the adult: a report of the American College of Cardiology/American Heart Association Task Force on Practice Guidelines (Writing Committee to Update the 2001 Guidelines for the Evaluation and Management of Heart Failure). *Journal of the American College of Cardiology* **46,** e1–e82 (2005) (cit. on pp. 1, 35, 36).
4. Heart Failure Society of America. HFSA guidelines for management of patients with heart failure caused by left ventricular systolic dysfunction—pharmacological approaches. *Journal of cardiac failure* **5,** 357–382 (1999) (cit. on p. 1).
5. Ponikowski, P., Voors, A., Anker, S., *et al.* 2016 ESC Guidelines for the diagnosis and treatment of acute and chronic heart failure: The Task Force for the diagnosis and treatment of acute and chronic heart failure of the European Society of Cardiology (ESC). Developed with the special contribution. *European Journal of Heart Failure* **18** (2016) (cit. on pp. 1, 2, 35, 37).
6. Engelfriet, P. M., Hoogenveen, R. T., Poos, M., *et al.* Hartfalen: epidemiologie, risicofactoren en toekomst. *RIVM rapport 260401006* (2012) (cit. on pp. 1, 31).
7. Mosterd, A. & Hoes, A. W. Clinical epidemiology of heart failure. *Heart* **93,** 1137–1146 (Sept. 2007) (cit. on p. 1).
8. MUSC Health Medical University of South Carolina. *Congestive Heart Failure* Sept. 2017 (cit. on p. 2).
9. Burns, K. V., Gage, R. M., Curtin, A. E. & Bank, A. J. Long-term echocardiographic response to cardiac resynchronization therapy in initial nonresponders. *JACC: Heart Failure* **3,** 990–997 (2015) (cit. on pp. 2, 54).
10. NVT/NVVC, W. *Rapport LVAD* Aug. 2014 (cit. on p. 3).
11. O'Brien, B. & Bruzzi, M. Shape memory alloys for use in medicine, 49–72 (2011) (cit. on p. 3).
12. Ryhänen, J. *Biocompatibility evaluation of nickel-titanium shape memory metal alloy* (Oulun yliopisto, 1999) (cit. on pp. 3, 44, 55).
13. Behl, M. & Lendlein, A. Shape-memory polymers. *Materials today* **10,** 20–28 (2007) (cit. on pp. 3, 46).
14. Abraham, W. T., Fisher, W. G., Smith, A. L., *et al.* Cardiac resynchronization in chronic heart failure. *New England Journal of Medicine* **346,** 1845–1853 (2002) (cit. on p. 4).

15.Sutton, M. G. S. J., Plappert, T., Abraham, W. T., *et al.* Effect of cardiac resynchronization therapy on left ventricular size and function in chronic heart failure. *Circulation* **107,** 1985–1990 (2003) (cit. on p. 4).

16.Gras, D., Leclercq, C., Tang, A. S., *et al.* Cardiac resynchronization therapy in advanced heart failure the multicenter InSync clinical study. *European journal of heart failure* **4,** 311–320 (2002) (cit. on p. 4).

17.Dynalloy, I. Technical characteristics of Flexinol actuator wires. *CA: Tustin* (2011) (cit. on pp. 5, 44–46).

18.Sengupta, P. P., Tajik, A. J., Chandrasekaran, K. & Khandheria, B. K. Twist mechanics of the left ventricle. *JACC: Cardiovascular Imaging* **1,** 366–376 (2008) (cit. on pp. 5, 30, 34, 54).

19.Loon, J. v., Luinstra, J. M., Schrader, I. M. W. & Velden, F. M. A. v. d. *Smart materials ter ondersteuning van een falend hart* June 2015 (cit. on p. 17).

20.Geervliet, E., Paalvast, A. & van Rheenen and M.A. Schreijer, B. S. *The use of a shape memory material in the treatment of heart failure with a reduced ejection fraction* June 2017 (cit. on p. 17).

21.Shiraishi, Y., Yambe, T., Saijo, Y., *et al. Morphological approach for the functional improvement of an artificial myocardial assist device using shape memory alloy fibres* in *Engineering in Medicine and Biology Society, 2007. EMBS 2007. 29th Annual International Conference of the IEEE* (2007), 3974–3977 (cit. on pp. 17, 45).

22.Velázquez, R. & Pissaloux, E. E. Modelling and temperature control of shape memory alloys with fast electrical heating. *Int. J. of Mechanics and Control* **13** (2012) (cit. on p. 18).

23.Kalogerakos, P. D., Hassoulas, J. & Ladopoulos, V. S. Beyond heart transplantation: Potentials and problems of the shape memory alloy fibers in the treatment of heart failure. *ASAIO journal* **60,** 263–268 (2014) (cit. on pp. 19, 45).

24.Bikson, M. A review of hazards associated with exposure to low voltages. *New York: University of New York* (2004) (cit. on p. 20).

25.DiMaio, D. & DiMaio, V. J. *Forensic pathology* (CRC press, 2001) (cit. on p. 20).

26.Al-Ahmad, A., Ellenbogen, K. A., Natale, A. & Wang, P. J. *Pacemakers and Implantable Cardioverter Defibrillators: An Expert's Manual* 3–18 (Cardiotext Publishing, LLC, 2010) (cit. on p. 20).

27.Mond, H. G. & Freitag, G. The cardiac implantable electronic device power source: evolution and revolution. *Pacing and Clinical Electrophysiology* **37,** 1728–1745 (2014) (cit. on pp. 20, 52).

28.Hassoulas, I. A., Ladopoulos, V. S. & Kalogerakos, P. Study of shape memory alloy fibers for the development of artificial myocardium. *Hellenic J Cardiol* **51,** 301–309 (2010) (cit. on p. 21).

29.Naish, J. *et al. Medical Sciences E-Book* (Elsevier Health Sciences, 2014) (cit. on p. 21).

30.Group, L. *Product: Cardiac Biosimulator Platform* Sept. 2017 (cit. on p. 22).

31.Klabunde, R. *Cardiovascular physiology concepts* 41–59 (Lippincott Williams & Wilkins, 2011) (cit. on pp. 25, 26).

32.Boron, W. F. & Boulpaep, E. L. *Medical physiology, 2e updated edition* 529–553 (Elsevier Health Sciences, 2012) (cit. on pp. 26, 27).

33.Marieb, E. N. & Hoehn, K. *Human anatomy & physiology* (Pearson Education, 2016) (cit. on p. 26).

34.Sidebotham, D. *Cardiothoracic critical care* 3–27 (Elsevier Health Sciences, 2007) (cit. on p. 27).

35.Naidu, S. S. Novel percutaneous cardiac assist devices. *Circulation* **123,** 533–543 (2011) (cit. on p. 28).

36.Rankin, J. S., Mchale, P. A., Arentzen, C. E., *et al.* The three-dimensional dynamic geometry of the left ventricle in the conscious dog. *Circulation Research* **39,** 304–313 (1976) (cit. on p. 29).

37.Sengupta, P. P., Korinek, J., Belohlavek, M., *et al.* Left ventricular structure and function. *Journal of the American College of Cardiology* **48,** 1988–2001 (2006) (cit. on p. 30).

38.Buckberg, G., Hoffman, J., Mahajan, A., Saleh, S. & Coghlan, C. Cardiac mechanics revisited. *Circulation* **118,** 2571–2587 (2008) (cit. on p. 30).

39.Greenbaum, R., Ho, S. Y., Gibson, D., Becker, A. & Anderson, R. Left ventricular fibre architecture in man. *British heart journal* **45,** 248–263 (1981) (cit. on p. 30).

40.Sengupta, P. P., Krishnamoorthy, V. K., Korinek, J., *et al.* Left ventricular form and function revisited: applied translational science to cardiovascular ultrasound imaging. *Journal of the American Society of Echocardiography* **20,** 539–551 (2007) (cit. on p. 30).

41.Holdrege, C. & Creeger, K. *The dynamic heart and circulation* 1–21 (Association of Waldorf Schools of North America, 2002) (cit. on p. 30).

42.Engelfriet, P., Poos, M. & Rutten, F. *Aantal nieuwe gevallen van hartfalen in de huisartsenpraktijk* Aug. 2017 (cit. on p. 31).

43.Van den Broek, S. in *Handboek hartfalen* 5–16 (Springer, 2011) (cit. on p. 32).

44.Kasper, D., Fauci, A., Hauser, S., *et al.* in *Harrison's principles of internal medicine* (2015) (cit. on p. 33).

45.Kumar, P. & Clark, M. in *Clinical medicine, 7th edn.* 681–810 (Elsevier, 2009) (cit. on p. 34).

46.De Jong, S. in *Handboek hartfalen* 39–51 (Springer, 2011) (cit. on p. 35).

47.Meijers, W., van der Velde, A. & de Boer, R. Biomarkers in heart failure with preserved ejection fraction. *Netherlands Heart Journal* **24,** 252–258 (2016) (cit. on p. 35).

48.Bogaert, J. & Taylor, A. *Primary Cardiomyopathies* 284–321 (Springer, 2012) (cit. on p. 35).

49.Kloosterman, M., Maass, A., Rienstra, M. & Van Gelder, I. Cardiac resynchronization therapy: who is a candidate and who is not? *Nederlands tijdschrift voor geneeskunde* **161,** D1142 (2017) (cit. on pp. 37, 38).

50.Bouwels, L. & Elders, J. in *Handboek hartfalen* 185–199 (Springer, 2011) (cit. on p. 37).

51.Registry, N. C. D. *Nationale rapportage 2015 & ACS Snapshotweken* 2015 (cit. on p. 38).

52.Chachques, J., Grandjean, P., Tommasi, J., *et al.* Dynamic cardiomyoplasty: a new approach to assist chronic myocardial failure. *Life support systems: the journal of the European Society for Artificial Organs* **5,** 323–327 (1987) (cit. on p. 38).

53.Hagège, A. A., Desnos, M., Fernandez, F., *et al.* Clinical study of the effects of latissimus dorsi muscle flap stimulation after cardiomyoplasty. *Circulation* **92,** 210–215 (1995) (cit. on p. 39).

54.Walsh, R. G. Design and features of the acorn corcap tm cardiac support device: the concept of passive mechanical diastolic support. *Heart failure reviews* **10,** 101–107 (2005) (cit. on p. 39).

55.Batista, R. J., Verde, J., Nery, P., *et al.* Partial left ventriculectomy to treat end-stage heart disease. *The Annals of Thoracic Surgery* **64,** 634–638 (1997) (cit. on p. 39).

56.Fukamachi, K., McCarthy, P. M. & Powell, B. The Myosplint implant procedure. *Operative Techniques in Thoracic and Cardiovascular Surgery* **7,** 90–102 (2002) (cit. on p. 40).

57.Birks, E. J. A changing trend toward destination therapy: are we treating the same patients differently? *Texas Heart Institute Journal* **38,** 552 (2011) (cit. on p. 40).

58.De Mol, B. & Lahpor, J. An artificial heart: bridge to transplantation or permanent? *Nederlands tijdschrift voor geneeskunde* **157,** A7102–A7102 (2013) (cit. on p. 41).

59.Huang, W. On the selection of shape memory alloys for actuators. *Materials & design* **23,** 11–19 (2002) (cit. on p. 42).

60.Duerig, T. W., Melton, K. & Stöckel, D. *Engineering aspects of shape memory alloys* (Butterworth-Heinemann, 2013) (cit. on p. 42).

61.Buehler, W. J., Gilfrich, J. & Wiley, R. Effect of low-temperature phase changes on the mechanical properties of alloys near composition TiNi. *Journal of applied physics* **34,** 1475–1477 (1963) (cit. on p. 42).

62.Follador, M., Cianchetti, M., Arienti, A. & Laschi, C. A general method for the design and fabrication of shape memory alloy active spring actuators. *Smart Materials and Structures* **21,** 115029 (2012) (cit. on p. 43).

63.Frenzel, J., Wieczorek, A., Opahle, I., *et al.* On the effect of alloy composition on martensite start temperatures and latent heats in Ni–Ti-based shape memory alloys. *Acta Materialia* **90,** 213–231 (2015) (cit. on p. 43).

64.Mantovani, D. Shape memory alloys: Properties and biomedical applications. *Jom* **52,** 36–44 (2000) (cit. on pp. 44, 45).

65.Patoor, E., Lagoudas, D. C., Entchev, P. B., Brinson, L. C. & Gao, X. Shape memory alloys, Part I: General properties and modeling of single crystals. *Mechanics of materials* **38,** 391–429 (2006) (cit. on p. 44).

66.Jani, J. M., Leary, M., Subic, A. & Gibson, M. A. A review of shape memory alloy research, applications and opportunities. *Materials & Design* **56,** 1078–1113 (2014) (cit. on p. 44).

67.An, L., Huang, W. M., Fu, Y. Q. & Guo, N. A note on size effect in actuating NiTi shape memory alloys by electrical current. *Materials & Design* **29,** 1432–1437 (2008) (cit. on p. 44).

68.Jun, H. Y., Rediniotis, O. K. & Lagoudas, D. C. Development of a fuel-powered shape memory alloy actuator system: II. Fabrication and testing. *Smart materials and structures* **16,** S95 (2007) (cit. on p. 44).

69.Buehler, W. J. & Wang, F. E. A summary of recent research on the Nitinol alloys and their potential application in ocean engineering. *Ocean Engineering* **1,** 105IN7109–108IN10120 (1968) (cit. on p. 44).

70.Ryhänen, J., Kallioinen, M., Tuukkanen, J., *et al.* In vivo biocompatibility evaluation of nickel-titanium shape memory metal alloy: Muscle and perineural tissue responses and encapsule membrane thickness. *Journal of Biomedical Materials Research Part A* **41,** 481–488 (1998) (cit. on p. 44).

71.Mihálcz, I. Fundamental characteristics and design method for nickel-titanium shape memory alloy. *Periodica Polytechnica. Engineering. Mechanical Engineering* **45,** 75 (2001) (cit. on p. 44).

72.Tozzi, P., Michalis, A., Hayoz, D., Locca, D. & von Segesser, L. K. Artificial muscle for end-stage heart failure. *Asaio Journal* **58,** 103–108 (2012) (cit. on p. 45).

73.Bertacchini, O. W., Lagoudas, D. C., Calkins, F. T. & Mabe, J. H. *Thermomechanical cyclic loading and fatigue life characterization of nickel rich NiTi shape-memory alloy actuators* in *Proceedings of SPIE* **6929** (2008), 692916 (cit. on p. 45).

74.Chikkamaranahalli, S., Vallance, R. R., Khan, A., *et al.* Precision instrument for characterizing shape memory alloy wires in bias spring actuation. *Review of scientific instruments* **76,** 065105 (2005) (cit. on p. 46).

75.Lendlein, A. & Kelch, S. Shape-memory polymers. *Angewandte Chemie International Edition* **41,** 2034–2057 (2002) (cit. on p. 46).

76.Langer, R. & Tirrell, D. A. Designing materials for biology and medicine. *Nature* **428,** 487 (2004) (cit. on p. 47).

77.Fu, Y., Huang, W., Luo, J. & Lu, H. *Polyurethane shape-memory polymers for biomedical applications* 167–195 (Elsevier, 2015) (cit. on p. 47).

78.Zhang, X., Xiong, Y., Chen, Y., *et al.* Investigation of shape memory alloy spring elastic coefficient based on varying applied currents in a cardiac assist device. *Journal of Mechanics in Medicine and Biology* **14,** 1450048 (2014) (cit. on p. 47).

79.Barr, M. Pulse width modulation. *Embedded Systems Programming* **14,** 103–104 (2001) (cit. on p. 48).

80.Riou, O., Berrebi, S. & Bremond, P. *Non uniformity correction and thermal drift compensation of thermal infrared camera* in *Proc. of SPIE Vol* **5405** (2004), 295 (cit. on p. 49).

81.Peura, R. A. & Webster, J. in *Medical instrumentation: application and design* 45–90 (John Wiley & Sons, 2010) (cit. on p. 50).

82.Giancoli, D. in *Physics for Scientists and Engineers with Modern Physics, 4th edn. Prentice Hall: Upper Saddle River* 651–676 (2009) (cit. on p. 52).

83.Roche, E. T., Horvath, M. A., Wamala, I., *et al.* Soft robotic sleeve supports heart function. *Science translational medicine* **9,** eaaf3925 (2017) (cit. on p. 53).

84.Loree, H. M., Bourque, K., Gernes, D. B., *et al.* The Heartmate III: design and in vivo studies of a maglev centrifugal left ventricular assist device. *Artificial organs* **25,** 386–391 (2001) (cit. on p. 53).

85.Najjar, S. S., Slaughter, M. S., Pagani, F. D., *et al.* An analysis of pump thrombus events in patients in the HeartWare ADVANCE bridge to transplant and continued access protocol trial. *The Journal of Heart and Lung Transplantation* **33,** 23–34 (2014) (cit. on p. 53).

86.Noon, G. P., Morley, D. L., Irwin, S., *et al.* Clinical experience with the MicroMed DeBakey ventricular assist device. *The Annals of thoracic surgery* **71,** S133–S138 (2001) (cit. on p. 53).

87.Wang, J. X., Smith, J. R. & Bonde, P. Energy transmission and power sources for mechanical circulatory support devices to achieve total implantability. *The Annals of thoracic surgery* **97,** 1467–1474 (2014) (cit. on p. 53).

88.Hill, M. R. *System and method for bi-ventricular fusion pacing* US Patent 6,871,096. Mar. 2005 (cit. on p. 54).

89.Davies, C. R., Fukumura, F., Fukamachi, K., *et al.* Adaptation of tissue to a chronic heat load. *ASAIO journal (American Society for Artificial Internal Organs: 1992)* **40,** M514–7 (1993) (cit. on p. 55).

90.Ghio, S., Constantin, C., Klersy, C., *et al.* Interventricular and intraventricular dyssynchrony are common in heart failure patients, regardless of QRS duration. *European Heart Journal* **25,** 571–578 (2004).